Volume 44 | Number 22 | 21 November 2015 | Pages 7921–8378

Chem Soc Rev

Chemical Society Reviews
www.rsc.org/chemsocrev

ISSN 0306-0012

ROYAL SOCIETY OF CHEMISTRY

REVIEW ARTICLE
Guihua Yu *et al.*
A chemistry and material perspective on lithium redox flow batteries towards high-density electrical energy storage

Chem Soc Rev

REVIEW ARTICLE

View Article Online
View Journal | View Issue

Cite this: *Chem. Soc. Rev.*, 2015, 44, 7968

A chemistry and material perspective on lithium redox flow batteries towards high-density electrical energy storage

Yu Zhao,†[ab] Yu Ding,†[a] Yutao Li,[a] Lele Peng,[a] Hye Ryung Byon,[c] John B. Goodenough[a] and Guihua Yu*[a]

Received 7th April 2015

DOI: 10.1039/c5cs00289c

www.rsc.org/chemsocrev

Electrical energy storage system such as secondary batteries is the principle power source for portable electronics, electric vehicles and stationary energy storage. As an emerging battery technology, Li-redox flow batteries inherit the advantageous features of modular design of conventional redox flow batteries and high voltage and energy efficiency of Li-ion batteries, showing great promise as efficient electrical energy storage system in transportation, commercial, and residential applications. The chemistry of lithium redox flow batteries with aqueous or non-aqueous electrolyte enables widened electrochemical potential window thus may provide much greater energy density and efficiency than conventional redox flow batteries based on proton chemistry. This Review summarizes the design rationale, fundamentals and characterization of Li-redox flow batteries from a chemistry and material perspective, with particular emphasis on the new chemistries and materials. The latest advances and associated challenges/opportunities are comprehensively discussed.

1. Introduction

The increasing need for greater amounts of electrical energy storage is driven by the need to provide greater flexibility and stability to cope with the increasing production of renewable energy. Electrical energy storage *via* potential energy, such as pumped hydro and compressed air storage, can be an attractive option for bulk energy storage with a low life cycle cost, though they are limited by site selection and require a large initial investment and lengthy construction. Electrical storage *via* kinetic energy, such as flywheels, offers high power but low energy. The largest group of technologies for electrical storage is electrochemical storage technologies that can efficiently store electricity in chemicals and reversibly release it on demand. As predicted by Joint EASE/EERA recommendations for European Energy Storage Technology Development Roadmap towards 2030,[1] electrochemical energy storage technologies represent one of the most promising potential for development to market-based deployment in a time horizon of 10–20 years. In general, electrochemical energy storage possesses a number of desirable features, including pollution-free operation, high round-trip efficiency, and flexible power and energy characteristics to meet different functions, long cycle life, and low maintenance. As one of the most widely used technologies for electrochemical energy storage, rechargeable batteries stand out as the most important candidate in many industrial and household applications for the new energy economy from sustainable sources.[2]

Batteries are inherently simple in concept, but have not yet departed substantially from the discovery of the first galvanic battery developed by Alessandro Volta in the 1800s. Till now, battery development has progressed incrementally mainly due to the limitation of electrode materials and battery design, together with other difficulties in developing suitable electrolytes and mastering the interfaces between the electrode materials and the electrolytes.[3–6] The number of commercially available rechargeable battery systems is relatively small, with aqueous electrolyte (lead/acid, redox flow, alkaline nickel/metal hydride) and lithium batteries dominating the market. Table 1 summarizes key performances of major commercialized conventional and advanced batteries. Lead/acid battery which uses lead redox couples in both electrodes was the first and the least expensive one developed so far, and though as the most commonly used secondary batteries, its utilization of the active material is far from 100%. Rechargeable alkaline batteries are the most used electrochemical storage devices after lead–acid systems. Like primary alkaline cells, they have a relatively high internal resistance,

[a] *Materials Science and Engineering Program and Department of Mechanical Engineering, The University of Texas at Austin, Austin, TX 78712, USA. E-mail: ghyu@austin.utexas.edu*
[b] *Institute of Functional Nano & Soft Materials (FUNSOM), Soochow University, 199 Ren-Ai Road, Suzhou Industrial Park, Suzhou, Jiangsu, 215123, China*
[c] *Byon Initiative Research Unit (IRU), RIKEN, Hirosawa 2-1, Wako, Saitama 351-0198, Japan*
† These authors contributed equally.

Table 1 Key performances of major commercialized conventional and advanced batteries

Battery type		Energy density		Specific power	Cycle life at	Efficiency	Working temperature
		W h kg^{-1}	W h L^{-1}	W kg^{-1}	80% DOD[a]	(%)	(°C)
Lead–acid	Flooded	25–40	60–100	140–350	200–1500	70–75	20–40
	Valve-regulated	30–40	80–100	140–300	300–1500	80–85	20–40
	Compressed	40–50	100	140–250	800–1500	70–85	20–40
Alkaline	Ni–Cd (high power)	25–40	130	500	800–1500	70–75	−40–50
	Ni–Cd (high capacity)	40–50	130	120–350	800–1500	70–75	−40–50
	Ni–Zn	60–80	200–300	500–1000	200–1000	60–65	0–40
	NiMH (high power)	40–55	80–200	500–1400	500–2000	70–80	0–45
	NiMH (high capacity)	60–80	200–350	200–600	500–2000	70–80	0–45
High temperature	Sodium–sulphur	103	150	100	4500	89	−20–45
Lithium	Li-ion (high power)	70–130	150–450	600–3000	800–3000	90–95	−20–60
	Li-ion (high capacity)	110–220	150–450	200–600	800–3000	90–95	−20–60
	Li Polymer	100–180	100	300–500	300–1000	90–95	−20–110
Flow batteries	High capacity	60–80	75–80	50–150	10 000	70–75	0–40
Electrochemical capacitors	High power	3–5	3–10	2000–10 000	> 500 000	95–100	−20–90
	High capacity	12–20	3–6	2000–10 000	> 500 000	95–100	−20–90

[a] Depth of discharge.

making them unsuitable for high-rate discharging. They also have limited cycling life if deeply discharged, and the available energy on each cycle decreases. Sodium–sulphur battery must have insulation and active heating to maintain a 300 °C operating point, or the resulting freeze thaw cycles and thermal expansion can lead to mechanical stresses, damaging seals and other cell components and possibly causing an explosion and fire. Conventional redox flow batteries based on aqueous-chemistry are of interest for stationary applications due to their modular design and potentially low cost. However, the limitations are obvious: low energy density originated from low working potential limited by electrolysis to *ca.* 1.5 V cell voltage, and low ion concentrations (typically 1–2 M), yielding only ~40 W h L^{-1} energy density for the fluids alone.[7] Even the prominent battery technologies such as the Li-ion battery still show large gaps between expected and practical performances.[8]

Breakthroughs in rechargeable battery technologies have been regarded as perhaps the most crucial need for future electrical energy storage, which wouldn't be realized with incremental improvements in existing technologies, but rather by the development of novel energy storage concepts incorporating new materials and chemical processes.[9–12] Li-redox flow battery represents such a new trend towards the design of next-generation alkali-ion battery with lower cost than conventional Li-ion batteries, and a voltage greater than conventional redox-flow battery based on proton chemistry. A Li-redox flow battery uses lightweight Li^+-ion as its charge carrier, and liquid phase redox reaction from redox molecule with relatively high redox potential as active material in the cathode, metallic lithium or soluble redox molecule with relatively low redox potential as active material in the anode. The amount of energy stored is determined by the amount of redox molecules, while power density is determined by redox kinetics of redox molecules and the rate of mass/charge transport inside the cell. Li-redox flow battery represents a promising electrical energy storage system for large-scale energy storage due to its modular design that provides flexible operation, transportability, and moderate manufacturing cost. In this Review, following an introduction of the operation principles and smart features of the Li-redox flow battery systems, recent advances, challenges, and possible solutions to this new battery system are discussed in detail.

2. Architecture and electrochemistry of Li-redox flow batteries

A battery cell is typically composed of two electrodes, which have different chemical potentials, and connected by an electrolyte. When these electrodes are connected by external circuit, electrons spontaneously flow from the more negative to the more positive potential. Ions are transported through the electrolyte, maintaining the charge balance, and electrical energy can be tapped by the external loading. The cell converts stored chemical energy into electrical energy *via* redox reactions at the redox centre of the anode and cathode. A variety of cells, primary and secondary, based on different redox chemistry have been realized though they are essentially the same technology.

One of the most important secondary batteries is redox-flow battery, which is designed to store energy on the medium to large scale, particularly in applications such as load levelling, power quality control and facilitating renewable energy deployment.[13] Unlike other secondary batteries that store electrical energy in solid electrode materials, the rechargeability of a redox-flow battery is provided by two chemical components with reversible redox behaviour dissolved in liquids contained within the system and external reservoirs.[7,14–17] The typical structure of a redox-flow battery, vanadium redox battery for instance (Fig. 1a), has two chambers, a positive chamber and a negative chamber, separated by an ion-exchange membrane. These two chambers are circulated with aqueous electrolytes containing active species in different valence states. The modular design distinguishes redox-flow battery from other solid-electrode-based electrochemical energy storage systems: decoupled energy capacity owing to the external circulating sub-system, and quick response arising from fast mass/charge transfer between the electrodes and intimate liquid–solid interface between active

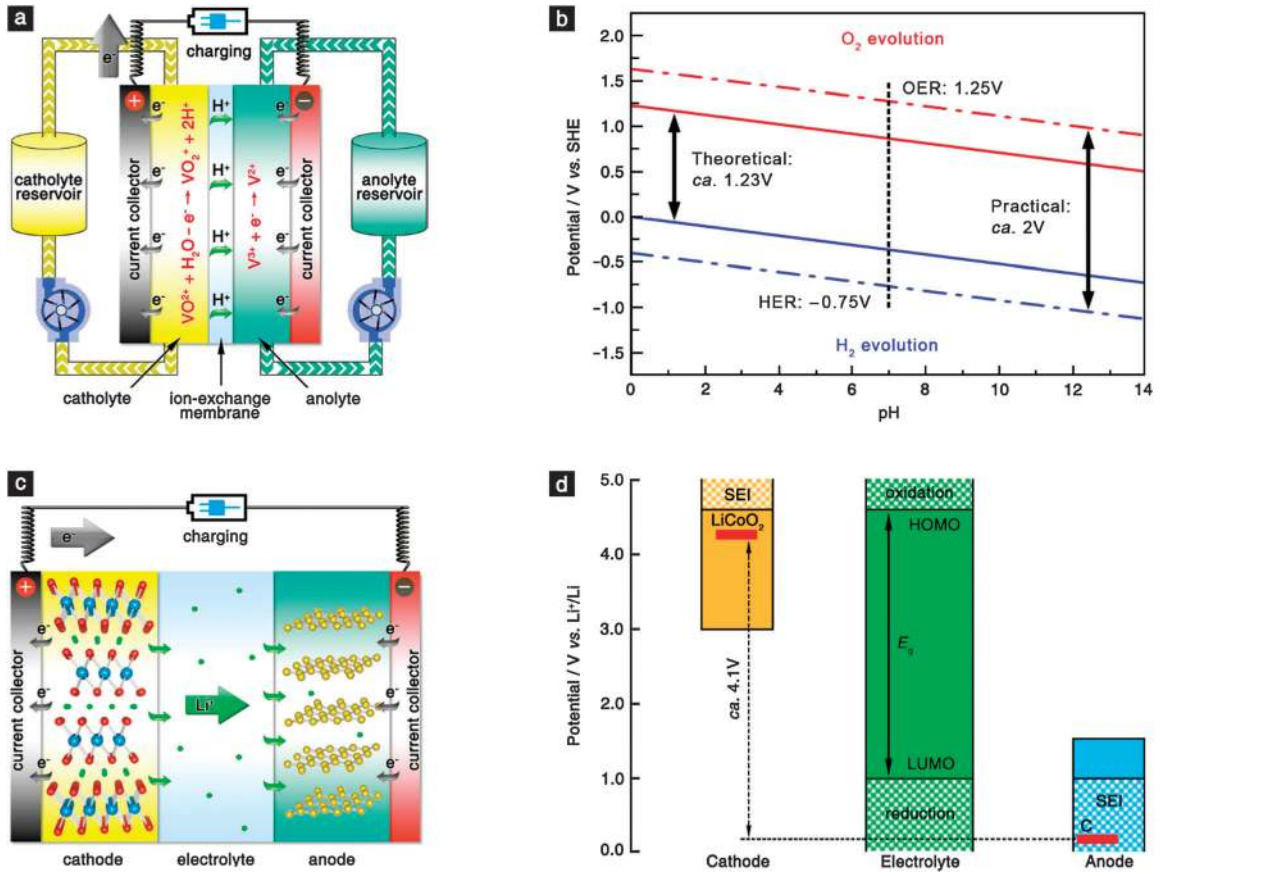

Fig. 1 Principles of secondary batteries based on aqueous and aprotic electrolytes. (a) Schematic of a vanadium redox-flow battery. The active species are dissolved in a strong acid. During charge process, VO^{2+} is oxidized to VO_2^+ at the positive electrode and V^{3+} is reduced to V^{2+} at the negative electrode. The protons transport across the ion-exchange membrane to balance the charge. (b) Potential window of water at room temperature. (c) Schematic of a typical Li-ion battery. Upon charging, Li ions are deintercalated from the Li-intercalation compound and intercalated into the graphite layers. The process is reversed on discharge. The electrodes are separated by an aprotic electrolyte that transports Li ions between the electrodes. (d) Schematic energy diagram of organic electrolyte. E_g is the window of the electrolyte for thermodynamic stability.

species and current collector.[18] The limitations of the redox-flow batteries are also obvious: low energy density and efficiency resulted from limited solubility of active species/internal shuttle effect, highly corrosive electrolytes, and low operating potential limited by water electrolysis. From the thermodynamic point of view, water can be directly used as electrolyte. The decomposition potential of water is dependent on its acidity (Fig. 1b). In theory, the potential window of water is only 1.23 V regardless of the acidity. However, the electrolysis would not generally proceed beyond this potential window since the electrical input must provide the full amount of enthalpy of oxygen and hydrogen evolution reaction, which broadens the threshold of water electrolysis to *ca.* −0.75–1.25 V *vs.* SHE at neutral pH environment. Therefore, a regular cell provides a relatively low operating voltage in the range of 1.2–1.6 V.[19]

Another important category of rechargeable batteries is the Li-ion battery and Li-ion polymer batteries. In a Li-ion battery (Fig. 1c), the positive electrode is a Li-intercalation compound, typically transition metal oxides or chalcogenides with stable crystal lattices that allow Li^+-ion to diffuse within their layer or tunnel structures,[20,21] whereas the anode is made of graphite in most commercialized Li-ion batteries.[22] The cathode and the anode are separated by aprotic electrolyte that allows Li^+-ions to move freely between the cathode and anode.[23] By injecting or extracting electrons, the redox reactions occur on the host lattice while mobile Li^+-ions reversibly intercalate into or deintercalate from the host matrix to compensate for electroneutrality. The adoption of organic electrolyte or solid electrolyte greatly broadens the potential window of a cell. The electrolyte should be electrochemically inert within the potential between the LUMO and the HOMO (Fig. 1d). An anode/cathode with redox potential below/above the LUMO/HOMO would reduce/oxidize the electrolyte unless a passivation layer (so-called solid electrolyte interface, SEI) creates a barrier to block electron transport from the anode/cathode to the electrolyte.[24] Therefore, thermodynamic stability requires locating the electrode redox potentials within the window of the electrolyte. Typically, carbonates show an oxidation potential at *ca.* 4.7 V[25] and a reduction potential near 1.0 V.[26] It's found that EC provides a stable SEI layer on the surface of a carbon anode that protects the electrolytes from further decomposition after SEI formation. Therefore, the commercial Li-ion cells based on

$LiCoO_2$ cathode and graphite anode can reach an average operating potential of 4 V.[10] Li-ion batteries and Li-ion polymer batteries presently have dominated the market of portable electronics, and possibly would be used in other areas where high energy density are needed, such as electric vehicles. However, it's difficult to increase the energy capacity in a packaged cell limited by the insertion chemistry of electrode materials. In addition, the power density is relatively low because of slow diffusion of Li^+ ions in the bulk electrode. Besides, the relatively high material cost might also be a critical obstacle for large-scale applications.

Li-redox flow battery is an emerging battery technology that combines the advantage of a redox-flow battery and a Li-ion battery. The structure of a Li-redox cell (Fig. 2) inherits the smart features of conventional redox-flow batteries: soluble cathode-active redox couple dissolved in a proper solvent to form the catholyte, and metallic Li as the anode or soluble anode-active redox couple dissolved in a proper solvent to form the anolyte. The catholyte and the anolyte can be stored in external reservoirs and circulated with the assistance of external circulating sub-system. Therefore, the energy capacity can be independently scaled up. The chemistry of a Li-redox cell shifts from proton-mediated redox reaction to a Li^+-mediated one, which provides sufficiently high operating voltage that is comparable to the Li-ion batteries. The charge transport inside the battery is based on the transport of Li ions between anode and cathode, and certain Li-ion conducting membranes are adopted to prevent the crossover of redox couples in either side of electrodes.

In a typical charge process, the reduced form of one redox species (Red1) in the catholyte is oxidized to its oxidized form (Ox1) at the positive electrode, and Li^+ or the oxidized form of another redox species (Ox2) in the anolyte is reduced to metallic Li or its reduced form (Red2) at the negative electrode, respectively. Li^+ ions diffuse across the Li^+-ion conducting membrane to balance the charge. This process usually proceeds until the redox species are exhausted in the electrolyte. General electrochemical reactions during charge process at the electrodes are shown below:

$$\text{Positive electrode: } C^{x+} - ye^- \rightarrow C^{(x+y)+}$$

$$\text{Negative electrode: } Li^+ + e^- \rightarrow Li$$

$$\text{or } A^{m+} + ne^- \rightarrow A^{(m-n)+}$$

$$\text{Overall reaction: } C^{x+} + yLi^+ \rightarrow C^{(x+y)+} + yLi$$

$$\text{or } nC^{x+} + yA^{m+} \rightarrow nC^{(x+y)+} + yA^{(m-n)+}$$

where $C^{(x+y)+}/C^{x+}$ and $A^{m+}/A^{(m-n)+}$ stand for the redox couple in the catholyte and the anolyte, respectively. The process is reversed on discharge.

Depending on the anode structure, Li-redox flow cells can be categorized into two types: full-flow Li-redox cell and semi-flow Li-redox cell. The former uses redox-active liquid or slurry as the catholyte and the anolyte.[19,27] The latter, which dominates current Li-redox flow battery research, uses redox-active liquid or slurry as the catholyte and Li metal as the anode.[18] Depending on the electrolyte used, Li-redox-flow cell can be divided into two categories: one uses aqueous/aprotic hybrid electrolyte configuration, and the other uses aprotic electrolyte configuration. The basic set-up of the prototype Li-redox flow cell with aqueous/aprotic hybrid electrolyte is essentially similar with conventional redox flow battery (Fig. 3). In the cathode or anode compartments, a porous conductive layer, usually made from graphitic materials,

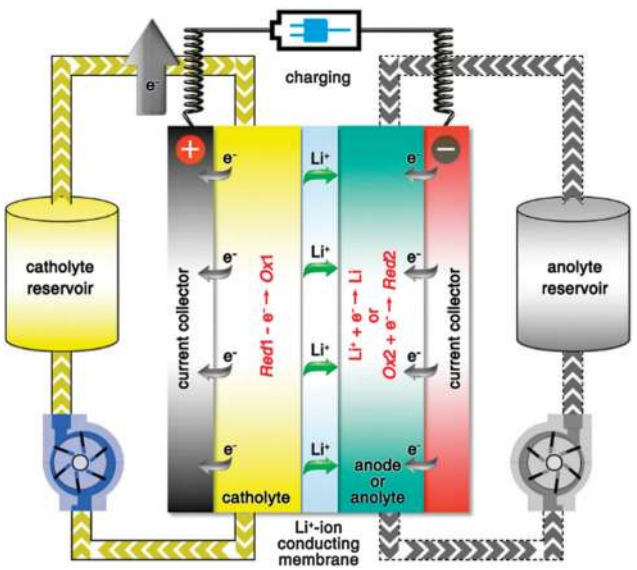

Fig. 2 Structure and working principle of a Li-redox flow cell.

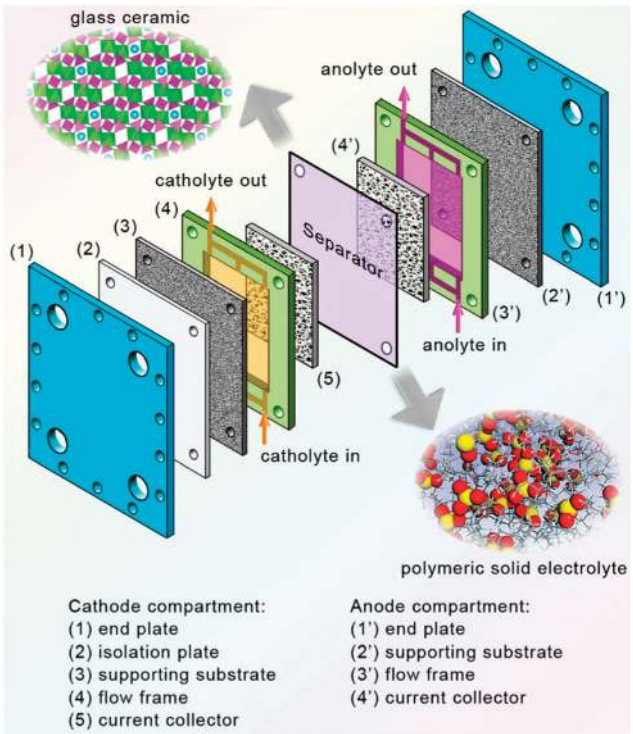

Fig. 3 Schematic structure of a Li-redox flow cell.

is applied as the diffusion layer and the current collector, and the catholyte or anolyte in the external reservoir can be pumped into the flow frame, and circled *via* eternal circuit. The thickness of the flow frame is usually about 1–3 mm, and the electrolyte flows through the electrode is normally laminar.[28] The Li-ion conducting glass ceramic or polymeric solid electrolyte can be used as separator to block the crossover between the catholyte and the anolyte. Particularly, metallic Li can be directly used as the anode taking advantage of its high energy density. In such a configuration, a buffer layer and conventional organic electrolyte are usually used to prevent corrosion of solid electrolyte by metallic Li and to facilitate Li^+-ion transport between metallic Li and solid-electrolyte separator.

3. Li-redox flow batteries in aqueous/aprotic hybrid electrolyte system

From the thermodynamic point of view, water can be directly used as the cathode in a lithium battery and demonstrates the overall reaction as shown in eqn (1).[29,30] The first patented primary Li-redox battery in aqueous/aprotic hybrid electrolyte system was proposed by PolyPlus Battery Company in 2007,[31] and several other primary Li-redox cells based on the similar chemistry have also been reported.[32,33] The first rechargeable Li-redox flow battery based on aqueous/aprotic hybrid electrolyte system was proposed by Goodenough's and Zhou's groups,[34,35] and further investigated by several other groups. In the initial proof-of-concept studies, iron-based redox couples, such as Fe^{3+}/Fe^{2+} and $Fe(CN)_6^{3-}/Fe(CN)_6^{4-}$, were used to construct rechargeable Li-redox flow batteries with metallic Li as the anode.

$$Li + H_2O \rightarrow LiOH + \tfrac{1}{2}H_2(g) \quad (1)$$

One of the key principles for construction of the Li-redox flow cells is the selection of cathode-active materials, which must satisfy a number of requirements: (i) both oxidized and reduced forms must be highly soluble to minimize the storage volume and mass and to allow high mass transfer rates and current densities; (ii) the formal potential of one couple must be highly positive, and the other highly negative to maximize the cell voltage and energy density; (iii) the heterogeneous reaction rate for the charging and discharging reactions at the inert electrodes should be rapid so that the electrode reactions occur at their mass transfer controlled rates; (iv) oxidized and reduced form should be stable, and this stability pertains to reaction with solvent, electrolyte, atmosphere, and electrode materials; (v) the materials should be safe, inexpensive, and abundant; (vi) the couple should not be corrosive and reactive with cell materials, or the storage vessel. Successful attempts have been achieved by using several reversible redox couples in aqueous phase, such as I_3^-/I^-,[36] Br_3^-/Br^-,[37] Cu^{2+}/Cu,[38] O_2/OH^-,[39] and S_4^{2-}/S^{2-}.[40] In principle, Na may be a better choice for such cell system in consideration of a lower cost. The challenge is that Na^+ ionic conductors at present are not stable in aqueous phase, and do not exhibit the exclusive selectivity for Na^+ ions. Redox-active materials suitable for constructing Li/Na-redox batteries with hybrid electrolyte system are summarized in Fig. 4.[41]

The other key lies in the separator membrane. Li-ion conducting NASICON-type $Li_{1+x+3z}Al_x(Ti,Ge)_{2-x}Si_{3z}P_{3-z}O_{12}$ glass ceramic, in most cases, is used to isolate the aqueous electrolyte and aprotic electrolyte. Such glass ceramic shows reasonable ionic conductivity ($\sim 10^{-4}$ S cm^{-1}) at room temperature. Such glass ceramic is stable against the organic electrolyte or aqueous electrolyte from weak acidic to weak alkalic (pH 3–10). However, the reduction of Ti^{IV} at low potential (occurs below 1.6 V *vs.* Li^+/Li) makes it unstable when in direct contact with metallic lithium. Therefore, a buffer layer usually is required to separate the glass ceramic from Li in long-term operation. Currently, the development of a suitable solid electrolyte with emphasis on ionic conductivity and stability of the solid electrolyte is still ongoing.

3.1 Iron-based Li-redox flow batteries

The Li-redox flow battery in aqueous/aprotic hybrid electrolyte system was first studied with Fe^{III}/Fe^{II} redox couple, because

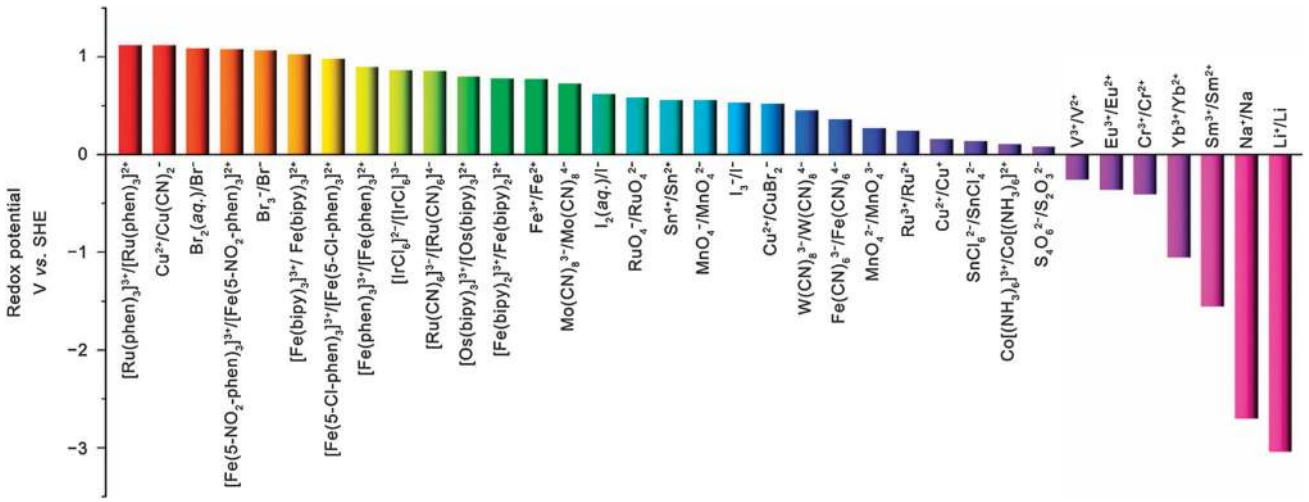

Fig. 4 Redox potential of various reversible redox couples suitable for constructing Li/Na-redox cells with aqueous/aprotic hybrid electrolyte system.

iron is an abundant and inexpensive element with many highly soluble compounds. In the proof-of-concept study, Goodenough and co-workers used an aqueous solution containing Fe^{3+} and Li salt as the catholyte to construct the static Li-redox cell.[34] At a relatively low current density, the cell could be discharged from 3.7 V to 3 V to reach the normalized capacity (Fig. 5a). However, the Fe^{3+}/Fe^{2+} redox couple only showed partial reversibility, mainly due to the hydrolysis of Fe^{3+} and Fe^{2+} in neutral pH environment that resulted in the formation of FeO(OH) and $Fe(OH)_3$ precipitates. To solve this problem, they used another redox couple, $Fe(CN)_6^{3-}/Fe(CN)_6^{4-}$, which undergoes reversible redox reactions in aqueous phase under neutral pH environment, and entails no making or breaking of Fe–C bonds. The cell could be galvanostatically discharged and charged with good Coulombic efficiency in the potential range of 3–3.75 V (Fig. 5b). The discharge voltage was stable between 3.3–3.5 V though slightly affected by the concentrations of the redox couple in the catholyte and the chelate effect of cyanide ligands. They further constructed the cell with a flow-through cathode,[42] offering a higher capacity and rate capability than its static counterpart. The discharge behaviour of the cell operating at cathode-flow mode was obviously improved compared to the static mode in terms of the stability of time-dependent discharge potential and energy density. Nevertheless, due to the limited solubility of $Fe(CN)_6^{3-}$ and $Fe(CN)_6^{4-}$, the energy density was too small to challenge the conventional redox-flow batteries.

Zhou and co-workers also introduced a Li-redox flow cell based on Fe^{3+}/Fe^{2+} redox couple. The cell used an acidic aqueous solution as catholyte (pH 1.7) to avoid the hydrolysis of ferric/ferrous ions.[35] In their strategy, the cell could be charged either through electric charging (Fig. 5c) or chemical charging by means of adding strong oxidizing agents to oxidize Fe^{2+} ions back to Fe^{3+} once the latter exhausted (Fig. 5d). They demonstrated that external oxidizing agents, such as $(NH_4)_2S_2O_8$ through eqn (2) and (3), could be utilized to oxidize the Fe^{2+} to Fe^{3+}, and the oxygen in the air might also be used to oxidize the discharge-product Fe^{2+} back to Fe^{3+}, despite the reaction was not fast enough to maintain a continuous discharge. In addition, the strong acidity/alkalinity of the catholyte would potentially destructure the solid electrolyte.[43] Thus the sustainability of this system need be further addressed.

$$S_2O_8^{2-} + 2H^+ + 2e^- \rightarrow 2HSO_4^- \quad \phi^0 = 2.123\ \text{V } \textit{vs.}\ \text{SHE} \qquad (2)$$

$$Fe^{3+} + e^- \rightarrow Fe^{2+} \quad \phi^0 = 0.771\ \text{V } \textit{vs.}\ \text{SHE} \qquad (3)$$

The advantages by using Fe^{3+}/Fe^{2+} redox couple for Li-redox flow battery rely in the proper redox potential and rich elemental abundance of iron. Challenges still remain such as the relatively low solubility of Fe-precursors compared with conventional redox-flow batteries,[16,44] the instability of solid electrolyte in strong acidic/alkalic catholyte,[45,46] and the sluggish kinetics of Fe^{3+}/Fe^{2+} redox couple ($\sim 10^{-5}$ cm s^{-1}).[15] Complexation of Fe^{3+} and Fe^{2+} may be a suitable solution to increase the redox potential of Fe^{III}/Fe^{II} couple and fasten the redox kinetics since the chemical principles related to the formation and properties of metal complexes are well developed and many new and potentially useful ligands have been reported. It can be seen from Table 2 that by using proper organic ligands, the redox potential of Fe^{III}/Fe^{II} redox couples can be tuned in a broad range between −1–0.8 V *vs.* SCE, and the redox kinetic constants also show orders of magnitude enhancement.[47–50]

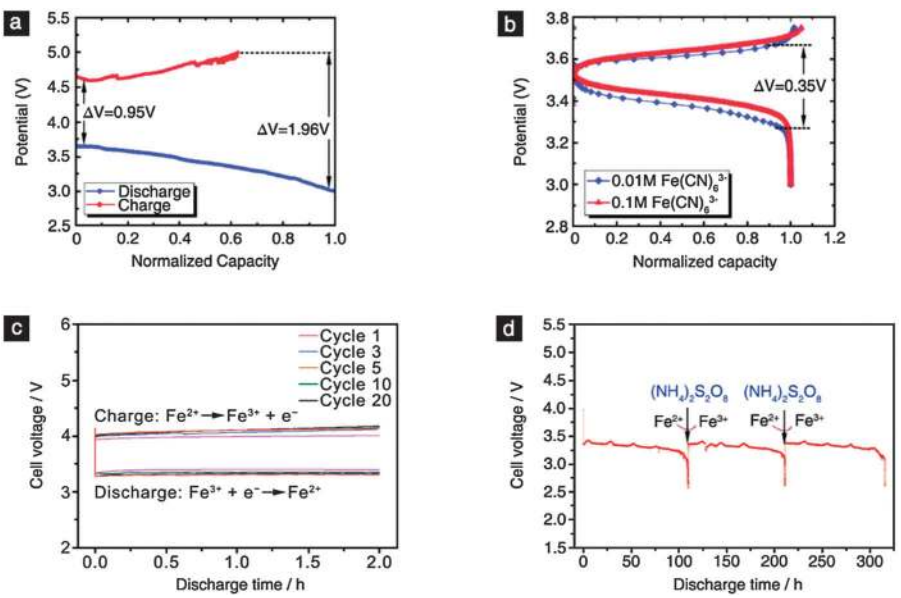

Fig. 5 Electrochemical performance of iron-based Li-redox flow batteries with aqueous catholyte. Charge/discharge profile of a Li-redox cell operated *via* Fe^{3+}/Fe^{2+} redox reaction (a), and $Fe(CN)_6^{3-}/Fe(CN)_6^{4-}$ redox reaction under different $Fe(CN)_6^{3-}$ concentration (b). Reproduced with permission from ref. 34. Copyright 2011, American Chemical Society. A demonstration of electric charging *via* Fe^{3+}/Fe^{2+} redox reaction (c) and chemical charging using $(NH_4)S_2O_8$ as oxidizer to chemically oxidize Fe^{2+} back to Fe^{3+} after fully discharge (d). Reproduced with permission from ref. 35. Copyright 2011, Wiley.

Table 2 Electrochemical parameters and solubility of Fe^{III}/Fe^{II} redox couples in aqueous phase

Ligands	ϕ^0 (V, *vs.* SCE)	k^0 (cm s^{-1})	Concentration (M)	Energy density (W h L^{-1})
2,9-Dimethyl-*o*-phenanthroline	0.82	2.5×10^{-2}	1.0	109.9
Bipyridine	0.82	5.6×10^{-2}	0.7	76.9
o-Phenanthroline	0.82	5.8×10^{-2}	0.8	87.9
Terpyridine	0.82	6.0×10^{-2}	0.3	33.0
Triethanolamine	−1.0	6.3×10^{-2}	0.6	35.1
Citrate	−0.21	N/A	1.8	148.1
Ethylenediaminetetraacetic acid	−0.10	4×10^{-3}	0.4	34.1
Cyanide	0.12	6.7×10^{-2}	1.0	91.1

3.2 Halogen-based Li-redox flow batteries

Halogen-based redox couples such as Br_3^-/Br^- and I_3^-/I^- show great potential in rechargeable Li-redox flow batteries owing to their relatively low molecular weight, highly reversible redox reaction, and proper redox potential. The reaction between metal halides and iodine, as well as the increased solubility of iodine in different solvents on addition of potassium iodide also attracted early attention in polyiodide chemistry. The solubility of iodine in aqueous phase is reasonably high when reacting with other iodides, which transform iodine to polyiodides (I_{2n+1}^-) with the triiodide ion (I_3^-) being the predominant specie (eqn (4)).[51] To date, a large number of polyiodide ions have been structurally characterized and anions in the range from I_2^- to I_{29}^{3-} have been established. Particularly, molten polyiodides show high electrical conductivity even at room temperature, and the reason for this behaviour is suggested to be similar with Grotthuss mechanism for protons in water. These properties suggest potential applications in a variety of areas, including fuel cells, batteries, solar cells, *etc.*[52] Bromine behaves similar with iodine in aqueous phase. Bromide ions can combine with bromine molecules to generate the tribromide ion (eqn (5)),[53] thus relatively high concentrations of Br^- and Br_2 can be utilized, leading to the enhancement of energy density. Br_3^-/Br^- redox couple shows rapid redox kinetics with good reversibility as a charge carrier, and it's potentially applicable in dye-sensitized solar cells, hydrogen–bromine fuel cell, zinc–bromine redox flow batteries, and alkali-ion batteries.[37,54–57]

$$I_2(s) + I^-(aq.) \rightarrow I_3^-(aq.) \quad K_{eq} = 752\ (25\ ^\circ C) \qquad (4)$$

$$Br_2(aq.) + Br^- \rightarrow Br_3^-(aq.) \quad K_{eq} = 14\ (25\ ^\circ C) \qquad (5)$$

The feasibility by using Br_3^-/Br^- and I_3^-/I^- redox reactions in aqueous phase relies on the proper redox potential that lies in water electrolysis window: only the reversible conversion between the valence state of −1 and 0 is allowed (Fig. 6a). In addition, good solubility that easily exceeds 1.5 M warrants a reasonable energy density several times higher than conventional redox flow batteries. Besides, the halogen-based catholyte undergoes rapid redox reactions with rate constant in the order of 10^{-3}–10^{-2} cm s^{-1} at room temperature,[37,58] considerably higher than those in conventional redox-flow batteries (10^{-3}–10^{-7} cm s^{-1}).[15] Furthermore, two electrons are transferred in Br_3^-/Br^- or I_3^-/I^- redox reaction, which means at a given concentration of the active materials, higher energy density can be achieved compared with those undergo single-electron transfer redox reaction. It can be seen that by using a 1.5 M bromine or iodine catholyte, the energy density exceeds 200 W h L^{-1} (Fig. 6b). In contrast, the energy densities for iron-based Li-redox flow battery with active-material-saturated

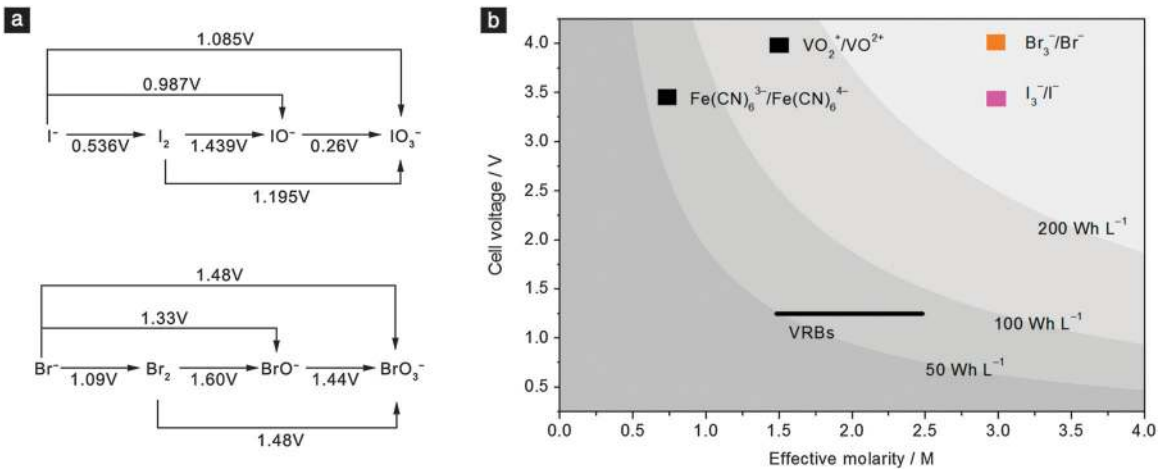

Fig. 6 (a) Redox potential of iodine and bromine at various valence states. All the redox potentials are standard values with respect to SHE. (b) Cell voltage, effective molarity and energy density of halogen-based Li-redox flow batteries. The corresponding parameters of conventional vanadium redox-flow batteries (VRBs) and iron-based Li-redox flow batteries are also included for comparison. The effective molarity stands for the concentration multiplied by the number of electrons involved in the redox reactions.

catholyte and conventional vanadium redox flow batteries are 60–70 and 50–90 W h L^{-1}, respectively (energy densities are calculated based on the catholyte and anolyte only).

The first iodine-based catholyte was first reported by Byon and co-workers.[36] The I_3^-/I^- redox couple based catholyte was prepared with 1 M of aqueous KI solution by the addition of I_2 to adjust the I_3^- concentration. Galvanostatic measurements showed ~80% Coulombic efficiency at room temperature on the first cycle of charge/discharge, and the initial Coulombic efficiency could be increased to ~100% either by preloading traces of lithium salt into the catholyte or increase the iodine concentration.[59,60] Both the cells with 0.08 M and 1 M I_2 showed impressive cyclability without capacity fading in 100 and 20 cycles, respectively. They demonstrated that a considerably high energy density could be achieved by using I_2-saturated catholyte, which delivered an energy density of 350 W h kg^{-1} (volumetric energy density of 700 W h L^{-1}) based on the total weight of the catholyte and the corresponding Li.

In the subsequent work, they further tailored the electrode structure by using nanostructured 3D current collector and equipped the cell with flowable cathode to improve the cycling stability and power density, and accelerate the diffusion of electroactive materials.[61,62] The 3D electrode architecture was constructed from a highly conductive, millimetre-thick vertically-aligned-carbon-nanotube mat (Fig. 7a).[62] The tailored cell exhibited stable cycling performance so that no capacity fading was observed for 200 fully charge/discharge cycles (Fig. 7b). The specific energy density reached ~330 W h kg^{-1} or ~650 W h L^{-1}, suggested the great potential for applications where high energy density are needed. In the flow cathode design, they used LiI aqueous solution to function as both the active material and supporting electrolyte.[61] The as-assembled Li-redox flow cell showed reasonably high power density of ~110 mW cm^{-2} at a current density of 40 mA cm^{-2} (Fig. 7c). Note that the current density is just comparable to most of conventional redox-flow batteries,[7] however, the power density should be at least twice higher considering the high discharge voltage around 2.8 V.

It's worth noting that I_3^-/I^- catholyte could be operated in natural pH environment, beneficial to maintain the structural stability of the solid electrolyte. The proper redox potential of 3.5 V *vs.* Li^+/Li and small polarization helped circumvent the electrolysis of water-based electrolyte. A critical issue of this Li-redox flow cell is the relatively small elemental abundance of iodine. Bromine may be another promising choice since the elemental abundance of bromine is three orders of magnitude higher than that of iodine.[41] Moreover, bromine tends to coordinate with other halides to form polybromide or hybrid polybromide in solution, significantly increasing its solubility. However, using Br^- directly as active material would result in quick fading of capacity and quick dropping of the discharge potential, which is attributed to the irreversible reaction between Br^- and BrO^-. Because the standard electrode potential of Br_2/Br^- is 1.09 V *vs.* SHE, only 0.24 V lower than that of BrO^-/Br^- if operated in natural pH environment. This is

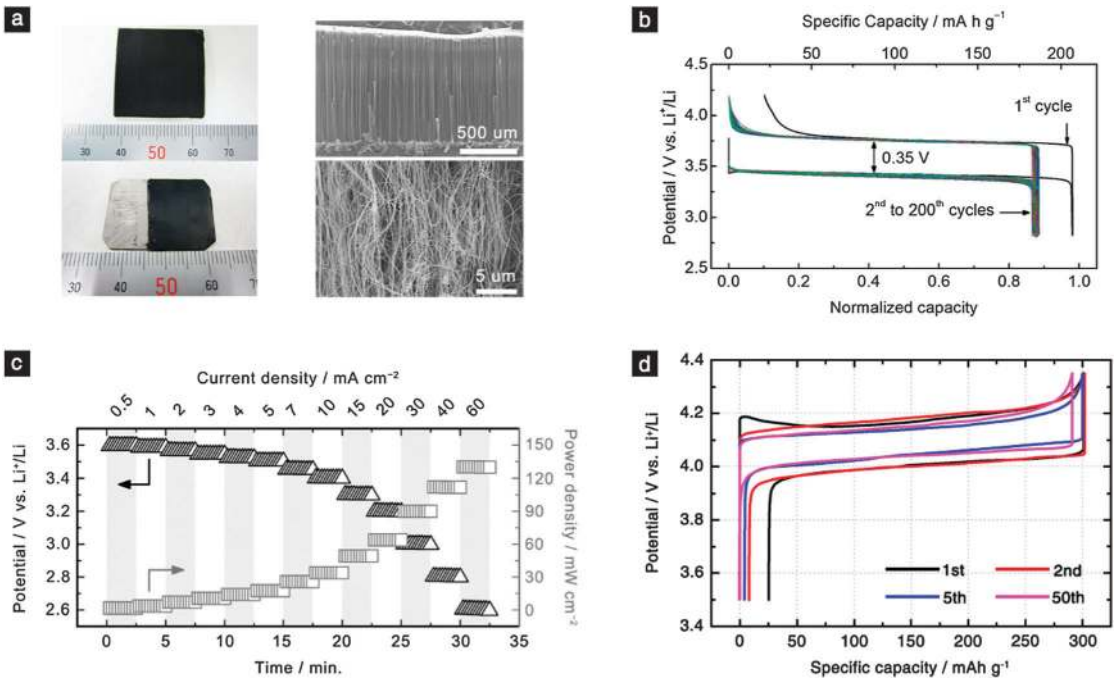

Fig. 7 Iodine-based Li-redox flow batteries. (a) Left panel: The vertically aligned carbon-nanotube mat grown on quartz (top) and transferred to Ti supporting substrate (bottom). Right panel: SEM images showing the microstructure of the 3D current collector. (b) Room-temperature charge/discharge profiles of a static Li-redox cell based on I_3^-/I^- catholyte at a current rate of 2.5 mA cm^{-2}. Reprinted with permission from ref. 62. Copyright 2014 American Chemical Society. (c) Potential and power density graphs using 1 M of LiI at 328 K. Reproduced with permission from ref. 61. Copyright 2013, Wiley. (d) Representative charge/discharge profiles of the Li-redox cell based on Br_3^-/Br^- catholyte with pH 4.5–5 at a current density of 0.1 C. Reproduced with permission from ref. 37. Copyright 2014, Royal Society of Chemistry.

different from the iodine case, in which the standard electrode potential of I_3^-/I^- (0.54 V *vs.* SHE) is *ca.* 0.45 V lower than that of IO^-/I^-. Possible solutions to exclude the reaction between BrO^- and Br^- include controlling the acidity of the catholyte to restrain the formation of BrO^-, and forming bromine complexes, such as tetrabutylammonium bromine, and *N*-methyl-*N*-ethyl morpholinium bromide to stabilize bromine during operation.[63]

Yu and co-workers first demonstrated a Li-redox cell with discharge potential at 4 V-level by using LiBr/KBr aqueous solution as the catholyte.[37] They found a proper acidity, pH 4.5–5 or lower, would effectively suppress the formation of BrO^-, therefore, the redox reaction between Br_2 and Br^- became the sole or dominant reaction in the catholyte. The practical threshold of O_2 evolution reaction potential was observed to be higher than 4.4 V *vs.* Li^+/Li while H_2 evolution reaction could only take place below 3 V *vs.* Li^+/Li in the catholyte. The typical discharge potential was $\sim$4 V *vs.* Li^+/Li and the reversible capacity reached $\sim$290 mA h g^{-1} (Fig. 7d). The capacity retention was stable with average capacity decay $<$0.1% per cycle, and the Coulombic efficiency was $\sim$100% after the first few cycles. Wu and co-workers also used Br_3^-/Br^- redox couple to construct a Li-redox cell.[57] In their design, a gel-type polymeric electrolyte composed of a sandwiched PVDF/glass fibre mat/PVDF membrane saturated by 1 M $LiClO_4$ EC/DEC/DMC solution was used as the buffer layer between Li metal and ceramic electrolyte.[64] The energy density was estimated to be $\sim$500 W h kg^{-1} assuming the catholyte weight up to 40–50% of the total weigh of a packaged cell.

Compared with other Li-redox flow batteries based on other catholyte chemistries, the catholytes using halogen-based redox couples show high discharge potential with large specific capacity. Iodine shows very high solubility in iodide aqueous solution, and I_3^-/I^- redox couple shows reliable reversibility, which in turn contribute to energy density and life-span of the Li-redox flow batteries. Moreover, the I_3^-/I^- redox reaction can proceed with good redox rate kinetics ($\sim10^{-2}$ cm s^{-1}) in neutral pH environment,[58] which is critical to maintain the structural stability of most water-stable ceramic electrolytes. The most critical issue with iodine-based catholyte lies in the low abundance of iodine elements. Bromine exhibits higher abundance and essentially provides higher redox potential than iodine. The redox rate kinetics ($\sim10^{-3}$ cm s^{-1}),[37] though an order of magnitude lower than that of iodine, still higher than those of conventional redox-flow batteries, and may be enhanced by surface treatments/functionalization of the current collector and assistance of catalytic species.[65,66] The cycling stability need be enhanced, and the side reactions or water electrolysis should be avoided. The toxicity of Br_2 and the highly complexing/corroding character of concentrated Br^- may pose limitation. The toxicity of Br_2 can be mitigated by proper use of complexing agents, but the effect of complexing agents on kinetics has not yet been studied quantitatively, particularly in acidic supporting electrolyte.

3.3 Chalcogen-based Li-redox flow batteries

Chalcogens such as oxygen and sulfur have gained considerable research interest owing to their high energy density and low cost. The rechargeable non-aqueous Li–O_2 cell was first reported by Abraham and co-workers,[67] and interest has expanded rapidly in recent years.[11] However, significant challenges remain such as dendrite formation and cycling efficiency of the Li anode, O_2 solubility, diffusivity and stability of the aprotic electrolyte, and the cathode that needs a membrane to block CO_2 and H_2O, while allowing O_2 to pass. Beyond the knowledge of Li–O_2 ad Li–S chemistry in aprotic electrolytes, pioneering work by Visco and coworkers opened up opportunity of the rechargeable O_2-based Li-redox flow batteries with aqueous/aprotic hybrid electrolyte.[68] It is generally understood that the battery chemistry consists of the reversible four-electron reduction/evolution of O_2 at the cathode and the Li^+/Li redox couple at the anode.[69] Compared with non-aqueous Li–O_2 cell which generally yields a discharge voltage around 2.7 V *via* a 2-electron process (eqn (6)), such a cell is capable to deliver higher discharge potentials, *ca.* 3.4 V and 4.2 V in alkaline and acidic catholyte, respectively (eqn (7) and (8)) *via* a 4-electron process. In addition, such cell is unnecessary to avoid ingress of H_2O from the atmosphere, which is one of the most critical factors to achieve stable cyclability of the non-aqueous Li–O_2 cells. Besides, the discharge product, primarily LiOH, is highly soluble in water, thus the cell does not need a current collector with large enough spare volumes to support solid Li_2O_2 formation as in non-aqueous Li–O_2 cells.

$$O_2(g) + 2Li^+ + 2e^- \rightarrow Li_2O_2 \quad \phi \approx 2.7 \text{ V } \textit{vs.} \text{ } Li^+/Li \tag{6}$$

$$O_2(g) + 2H_2O + 4e^- \rightarrow 4OH^-(aq.) \quad \phi^0 = 0.401 \text{ V } \textit{vs.} \text{ SHE} \tag{7}$$

$$O_2(g) + 4H^+(aq.) + 4e^- \rightarrow 2H_2O \quad \phi^0 = 1.229 \text{ V } \textit{vs.} \text{ SHE} \tag{8}$$

For the Li-redox flow cell with alkaline catholyte, the most utilized supporting salts is LiOH with the co-existence of $LiClO_4$, $LiNO_3$ or LiCl, which in turn provides alkaline environment to facilitate the ORR reaction and proper Li^+ conductivity. One key challenge in such cell is CO_2 ingression, resulting in the formation of Li_2CO_3, which is hard to decompose below the upper threshold potential range of the alkaline catholyte. As a result, it is necessary to apply a protective membrane to the outer surface of the cathode that permits O_2 diffusion while blocking CO_2, or to remove the latter from the atmosphere around the cell. Another key challenge is strong alkali environment in which the solid electrolyte becomes unstable. Imanishi and co-workers found that by using LiCl-saturated LiOH–H_2O solution, the dissolution of LiOH could be greatly suppressed owing to the high concentration of Li^+.[70] Such a solution showed moderate pH value of 7–9, suitable for the NASICON-type glass ceramic membrane. From the point view of a practical Li-redox flow cell, the use of concentrated LiCl in the catholyte may suffer from Cl_2 evolution or ClO^- formation during the high voltage charge process, and decreases the available amount of LiOH for the electrochemical process in the catholyte. The third key challenge would be the exploration of OER/ORR catalysts that are truly effective, long-lasting and inexpensive. Some non-noble catalysts, such as carbon-based materials, transition-metal oxides, *etc.*, have shown the capability to catalyze the OER and/or ORR in alkaline catholyte. Zhou and co-workers utilized graphene oxide nanosheets as ORR catalyst

and the air-electrode, and showed a high discharge voltage close to that of the 20 wt% Pt-loaded carbon black.[39] Due to the absence of effective OER catalyst, the cell only showed some rechargeability with large polarization similar to that of the Li–O_2 batteries with aprotic electrolyte. In addition, the corrosion on the air-electrode due to carbon oxidation in the charge process became more seriously during repeated charge, thus resulting in gradually increased polarization of the charge/discharge potentials.[71]

For the Li-redox flow cell with acidic catholyte, weak acid with high dissociation constant, such as HOAc/LiAc and H_3PO_4/LiH_2PO_4 buffer solution, is preferred to serve as the active material.[33,72,73] Strong acidic solution with proton-trapping additives such as imidazole, a small molecule with a strong ability to absorb the protons in water, may also serve as acidic catholyte for the Li-redox flow cell.[74] Though CO_2 ingression becomes less severe in the acidic catholyte, challenges still remain, such as acid concentration-dependent energy density of the catholyte, and the instability and low activity of non-noble metal catalysts as well as NASICON-type glass ceramic membrane in an acidic environment. Currently, the most widely used catalyst in Li-redox flow cell with acidic catholyte is Pt/C, which serves as both OER and ORR catalyst. Other promising non-noble metal catalysts include heterocyclic N compounds and compounds with transition metals coordinated to heterocyclic N for ORR,[75] and Ru, Sn, and Ir mono and bimetallic oxide materials for OER in acidic environment.[76]

Promising strategies to promote the performance of O_2-based Li-redox flow batteries either with acidic or alkali catholyte would be to develop bi-functional OER/ORR catalysts,[77,78] or decouple the ORR and OER electrodes.[79,80] Shao-Horn and co-workers used bi-metallic noble metal nanoparticles as a bi-functional catalyst to reduce the voltage gap between the ORR and OER with Au to enhance the ORR and Pt to lower the OER voltages.[81] They also showed that transition-metal oxoperovskites containing surface cations with an e_g^1 electron configuration and good bulk electronic conductivity give a fast ORR or OER in alkaline solution.[82,83] Perovskite $Sr_{0.95}Ce_{0.05}CoO_{3-\delta}$ loaded with copper nanoparticles could also serve as a bi-functional catalyst for ORR and OER in aqueous solution.[84] Dai and co-workers reported a hybrid material composed of Co_3O_4 nanocrystals grown on reduced graphene oxide (Fig. 8a) as a high-performance bi-functional catalyst for OER and ORR in alkali environment.[85] In their investigation, it was found that Co_3O_4 or graphene oxide alone has little catalytic activity. However, their hybrid exhibits similar ORR catalytic activity that could be further enhanced by the nitrogen-doping of graphene, but superior stability compared to Pt in alkaline solutions (Fig. 8b). The same hybrid was also found to shown highly active for the OER. They supposed such an enhancement was resulted from the synergetic chemical coupling effects between Co_3O_4 and graphene.

The concept of decoupling the ORR and OER electrodes has been demonstrated previously in metal hydride–air batteries,[80] and, in principle, can be applied in O_2-based Li-redox flow batteries. Manthiram and co-workers reported an O_2-based Li-redox cell using mesoporous $NiCo_2O_4$ nanoflakes grown on

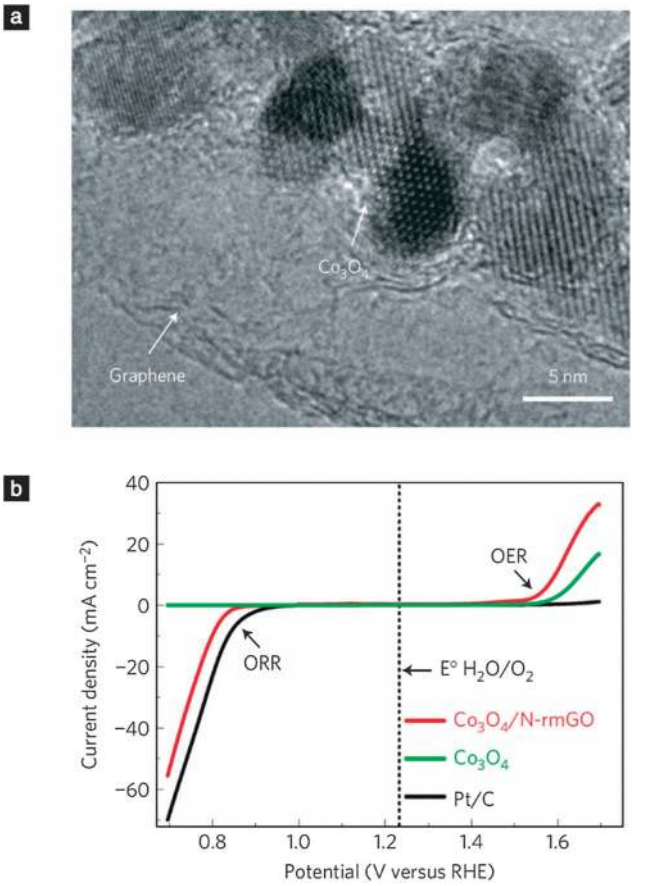

Fig. 8 Bi-functional OER/ORR catalysts. (a) TEM images of Co_3O_4/N-rmGO hybrid (N-rmGO: N-doped reduced mildly oxidized graphene oxide). (b) Oxygen electrode activities within the ORR and OER potential window of Co_3O_4/Co_3O_4/N-rmGO hybrid, Co_3O_4 nanocrystal and Pt/C catalysts dispersed on carbon fibre paper in O_2-saturated 0.1 M KOH. Reproduced with permission from ref. 85, Copyright 2011, Macmillan Publishers Limited.

nickel foam and N-doped mesoporous carbon loaded onto a hydrophobic carbon paper, respectively, as the decoupled ORR and OER electrodes (Fig. 9). The Co^{4+}/Co^{3+} couple is known to be a good OER catalyst, while the large surface area of mesoporous carbon along with N-doping provides a large number of catalytic sites, which lower the overpotential of ORR. Therefore, the cell showed stable cyclic performance with only 0.08 V increase in round-trip overpotential in alkali catholyte.[86]

$$3S_4^{2-} + 2e^- \rightarrow 4S_3^{2-} \quad \phi^0 = 2.563 \text{ V } \textit{vs.}\ Li^+/Li \qquad (9)$$

$$2S_3^{2-} + 2e^- \rightarrow 3S_2^{2-} \quad \phi^0 = 2.535 \text{ V } \textit{vs.}\ Li^+/Li \qquad (10)$$

$$S_2^{2-} + 2e^- \rightarrow 2S^{2-} \quad \phi^0 = 2.516 \text{ V } \textit{vs.}\ Li^+/Li \qquad (11)$$

The rechargeable non-aqueous Li–S cell have many attractive features such as natural abundance and low cost of sulfur, and high theoretical energy capacity. A critical problem inherent in the cell chemistry would be the formation of soluble polysulfides, which results in shuttle effect thus decreases the efficiency and cycling stability. Sulfur-based Li-redox flow battery, taking advantage of the redox reactions between S_4^{2-} and

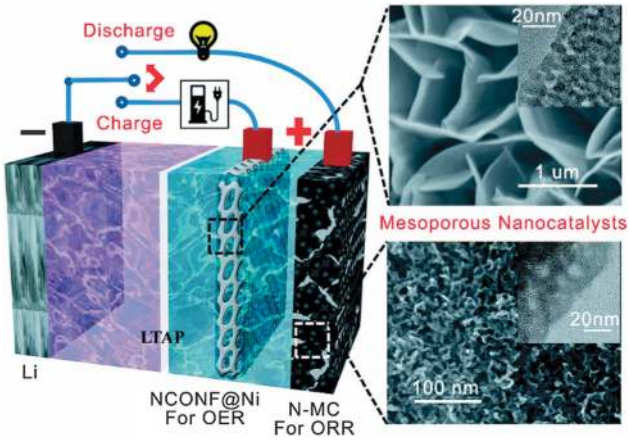

Fig. 9 Schematic of the decoupled electrodes loaded with mesoporous nanocatalysts. The upper-right SEM and TEM images showing the mesoporous $NiCo_2O_4$ nanoflakes directly grown onto nickel foam (NCONF@Ni) as the OER catalyst; the lower right SEM and TEM images shows the N-doped mesoporous carbon (N-MC) as the ORR catalyst. Reproduced with permission from ref. 86, Copyright 2014 Royal Society of Chemistry.

S^{2-} in aqueous phase as reported recently by Zhou and co-workers,[40] has shown its potential due to its high energy density up to 650 W h kg^{-1}. The reversible capacity based on the reaction between Li_2S_4 and Li_2S (shown in eqn (9)–(11)) could reach 1000 mA h g^{-1} with an average discharge voltage of 2.5 V. It's necessary to point out that the catholyte should be a strong alkali solution in order to lower the hydrogen evolution potential; the solubility of the oxidized form of S_2^{2-}, S_3^{2-} and S_4^{2-} in aqueous phase should also be considered.

3.4 Dye-sensitized photoelectron-synthetic Li-redox flow cell

The sun provides nearly unlimited energy. In order to serve as a primary energy source, solar energy has to be paired with an energy storage capability. This leads to the concept of "*solar fuels*" that targets water splitting into H_2 and O_2, and/or water reduction of CO_2 into almost any form of reduced carbon. Inspired by "*dye-sensitized solar cell* (*DSSC*)" as an energy generation device,[87] the concept of "*solar fuels*" has been achieved by a "*dye-sensitized photoelectrosynthesis cell* (*DSPEC*)" (Fig. 10a).[88–90] In such a cell, one electrode compartment of such cell is a spatially separated photoanode for water oxidation and the other electrode compartment is a physically separated cathode for CO_2 reduction. The two electrode compartments are separated by a proton exchange membrane, which allows for proton diffusion and charge balance. Such a device convert the solar energy into primary energy source, but lack the functionality to convert the formed solar fuels into electrical energy.

Li-redox flow cell with proper structural modification, namely a "*dye-sensitized photoelectrosynthetic Li-redox flow cell* (*DPLFC*)" can serve as a multifunctional device that combines energy generation, storage and conversion as a whole. It utilizes the photoanode of a conventional DSSC to generate current flow inside the cell from the solar irradiation, and two redox couples to store the generated energy as chemical energy, and converse the stored chemical energy into electrical energy

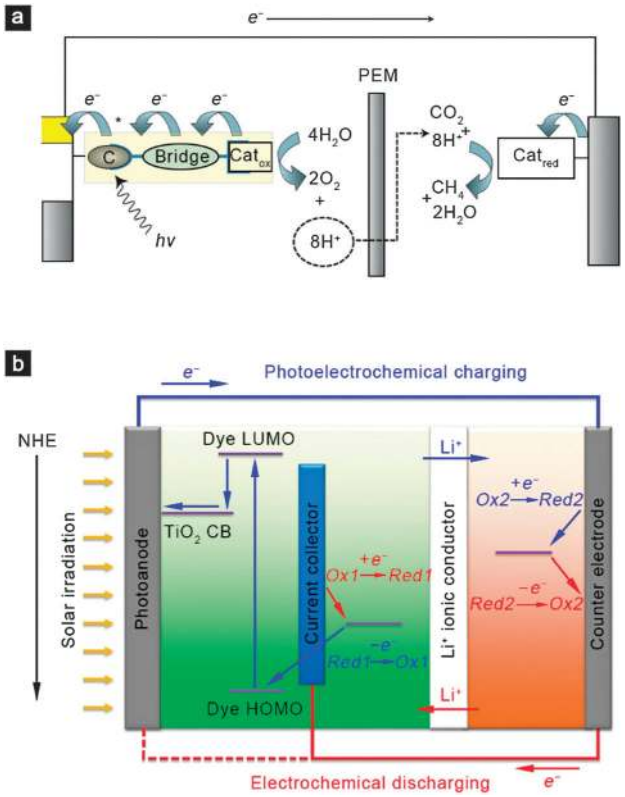

Fig. 10 (a) Schematic of a dye-sensitized photoelectrosynthesis cell (DSPEC). A DSPEC combines a molecular light absorber (chromophore C), bound to a semiconductor surface, with catalysts for water oxidation and carbon dioxide reduction, in an electrochemical cell. Light absorption gives a localized molecular excited state, which injects an electron into the conduction band of the semiconductor. This triggers a sequence of electron transfer events, which subsequently activate the catalysts. The bridge is an intervening electron transfer spacer that may be necessary to increase the distance between Cat_{ox} and the electrode to slow down back electron transfer. PEM is a proton exchange membrane for equilibrating protons between the two half reactions. Reproduced with permission from ref. 89, Copyright 2011, IUPAC. (b) General structure and working principle of a DPLFC.

through a Li-redox flow cell design. The general structure of a DPLFC is composed of three major parts: a photoanode responsible for solar energy capture, the catholyte/anolyte that converts the captured solar energy into chemical energy *via* the cathode/anode-active redox couples, and an ion-selective membrane for charge balance (Fig. 10b). Two independent processes are involved in the DPLFCs: the photoelectrochemical charging process and the electrochemical discharging process. During the photoelectrochemical charging process, taking a conventional TiO_2-based photoanode as example, electrons are excited from the HOMO to the LUMO of the dye molecules and the excited dye molecules oxidize the reduced form of the cathode-active redox mediator (Red1 $- e^- \rightarrow$ Ox1). Then the electrons are injected to the conduction band (CB) of the TiO_2 photoanode, and move through external circuit into the counter electrode to reduce the oxidized form of anode-active redox mediator (Ox2 + $e^- \rightarrow$ Red2). Simultaneously, Li^+-ions move from the photoanode side to the counter electrode side through the Li^+ ionic

conductor to balance the charge and sustain a continuous current flow. During the electrochemical discharge process, the reduced form of anode-active redox mediator is oxidized (Red2 − e^- → Ox2) on the counter electrode, and the electrons move back to the photoanode side through the external circuit to reduce the oxidized form of cathode-active redox mediator (Ox1 + e^- → Red1), either at the photoanode or through the third electrode. Meanwhile, Li^+-ions move back from the counter electrode side through the Li^+ ionic conductor.

The discharge potential of the DPLFC is determined by the potential difference between the anode-active and cathode-active redox mediators, and the potential of both the anode-active and cathode-active redox mediators should be located between the conduction band of TiO_2 and the HOMO of the dyes. The most widely used redox mediator in the photoanode side is I_3^-/I^-,[91] other redox mediators such as Br_3^-/Br^-, $(SCN)_3^-/SCN^-$ and $(SeCN)_3^-/SeCN^-$ have been tested with some success.[92] Generally, the conduction band of TiO_2 and the redox potential of cathode-active redox mediator, usually I_3^-/I^-, is −0.5 V and 0.3–0.4 V *vs.* SHE, respectively. Therefore, a potential with theoretical limitation of ~0.8 V can be expected from the DPLFC.

Gao and co-workers demonstrated a DPLFC using I_3^-/I^- propylene carbonate solution/Li_2WO_4 aqueous solution as the catholyte and anolyte, respectively.[93] Two pairs of redox peaks at 0.21/−0.27 V and −0.19/−0.58 V *vs.* Ag^+/Ag were observed for the cathode-active LiI in propylene carbonate electrolyte. While only one pair of redox peaks was observed for the anode-active Li_2WO_4 at 0.26 V/−0.16 V *vs.* Ag^+/Ag. The different redox potentials yielded a sloped discharge profile with the average working potential of ~0.45 V, corresponding to the average potential difference between the I_3^-/I^- and $WO_4^{2-}/WO_4^{(2+x)-}$ redox couples. With the same cell configuration, they further used quinoxaline as anode-active material in aqueous phase, and obtained a total energy conversion efficiency about 1.2%.[94]

To further understand the photoelectrochemical and electrochemical processes related to the device performance, reaction kinetics should be viewed based on the energy level diagram of the photoanode proposed by Hupp and co-workers[95] together with the reaction kinetics in the counter electrode. The kinetic processes on energy level diagram in DPLFC is proposed in Fig. 11. It appears that the most critical parameter to enhance the overall efficiency of a DPLFC is to use anode-active redox mediator with faster response time for charge injection from the counter electrode than the competing process, the charge injection from the TiO_2 CB into the conducting oxide substrate. Also, it's necessary to use cathode/anode-active redox mediator with higher/lower redox potentials that locate between the TiO_2 CB and the HOMO of the dyes to maximize the operating potential during electrochemical discharge. Other factors should be also considered such as developing new super chromophores that can collect light more efficiently than existing ones, new shuttles that can regenerate dyes at low driving force yet exhibit slow interception of injected charges, or new photoelectrode materials and architectures. The current generated by the photoanode is in the order of 10 mA cm^{-2}, which is several times higher than the maximum current density provided by the solid electrolyte

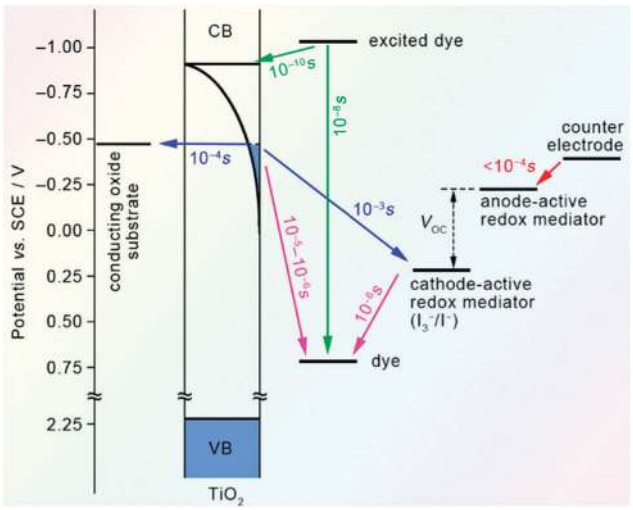

Fig. 11 Kinetic processes on energy level diagram in DPLFC.

without serious polarization. Therefore, the structural stability of the solid electrolyte under such a high current polarization needs further investigation. The DSSC usually yield an open circuit voltage around 0.7 V and the concentration of the redox species in the electrolyte usually below 0.2 M, which are the main obstacle to achieve reasonable energy density.

4. Li-redox flow batteries in aprotic electrolyte system

Li-redox flow batteries based on aqueous catholyte is potentially advantageous owing to the low cost of aqueous electrolytes and good solubility of redox-active inorganic or organometallic complexes. Aside from water electrolysis within a small potential window, most of current Li-redox flow batteries use strong acidic or alkaline catholytes, which raises serious concern about the durability of the glass ceramics. Employing aprotic electrolytes is considered as the primary advantage of Li-redox flow batteries over their aqueous counterpart, and also increases choices of available redox couples. Besides, employing aprotic electrolytes would potentially alleviate the corrosion on battery components, such separator and current collector in addition to a wider electrochemical window provided by the aprotic electrolytes. Moreover, the safety concern on the reaction between metallic Li and water resulted from the possible perpetration of aqueous electrolyte can also be alleviated since metallic Li was found to be stable in a number of aprotic solvents despite its reactivity.[25] Note that challenges still remain in employing aprotic electrolyte. It's necessary to address the relatively lower diffusion efficiency of the active materials and higher costs compared to their aqueous counterpart, and other unfavourable physical properties including moisture sensitivity, flammability, toxicity and solvent-dependent redox behaviours.[96]

The majority of the reported non-aqueous redox flow batteries are from anion-exchange systems where the active materials are usually composed of metal complexes with transition metals being

the redox centre.[97] Bipyridine[98,99] and acetylacetonate[100–102] coordinated transition metal complexes are the most intensively studied active materials in non-aqueous redox flow batteries. The major problems of non-aqueous redox flow batteries are the poor rate capability which arises from the poor redox kinetics, low energy efficiency due to the limited capability of the membrane to avoid the crossover of the electroactive materials, and significant capacity degradation over cycling. Recently emerging aprotic Li-redox flow batteries have attracted considerable research interest owing to their greatly enhanced characteristics over non-aqueous redox flow batteries, such as high discharge voltage, good round-trip efficiency and stable cyclability. Some new approaches have been proposed. For example, the semi-solid lithium rechargeable flow battery uses conventional Li-ion battery electrode materials in a form of suspension flowing through the flow battery configuration.[27] Properly protected Li anode is used to construct a membrane-free Li-redox flow battery with highly soluble polysulfides as cathode-active material.[103] Li-redox flow battery based on hybrid aprotic electrolytes provides the capability to maximize the redox potential and kinetics of metallorganic compounds.[104] These approaches take advantage of Li-ion battery in an attempt to inherit its high energy density, while adopt a flow battery configuration to decouple the power and energy. The synergy between the non-aqueous redox flow battery configuration and Li-ion battery chemistries has offered a fascinating new area for scientific research and has attracted more and more interest and effort.

4.1 Metallocene-based Li-redox flow batteries

Metallocene is a compound typically consisting of two cyclopentadienyl anions (Cp, $C_5H_5^-$) bound to a metal centre in the valence state of +2, with the resulting general formula $MII(C_5H_5)_2$. With the MCp_2 structure, they are sandwich complexes in which the two Cp rings are parallel. The sandwich MCp_2 structure is very robust with variable number of d electrons of 18 (Fe, Ru, Os). The neutral metallocenes of the 1st-row with 15 to 20e$^-$ (V, Cr, Mn, Fe, Co, Ni) correspond to the filling of the 5d orbitals split in three molecular orbital levels (e_{1g}: bonding, double; a_{1g}: non-bonding, simple; e^*_{1g}; antibonding, double) under the influence of the pseudo-octahedral field of the two Cp ligands.[105] A key property of metallocene is their ability to exist in the form of various oxidation states with sandwich structure and a variable number of d electrons between 14 and 20, even if the stability decreases as the variable number of d electrons is further away from 18. The oxidation or reduction is reversible and occurs without structural change. The redox potential of metallocenes and their derivatives is solvent-dependent, and certain metallocenes and their derivatives exhibit reversible or quasi-reversible redox behaviours. Table 3 lists the redox potential and reversibility of certain metallocenes.[106–112]

Among various metallocenes and their derivatives, ferrocene and its derivatives are the most widely studied in Li-ion batteries. Golovin and co-workers found ferrocene and its derivatives to be an effect electrolyte additives for overcharge protection of Li-ion batteries.[113] Ferrocene and its derivatives gave cell overcharge voltages that match closely with their redox potentials, and the cycle life of cells containing such additives generally was not adversely affected. Park and co-workers proposed to use chemically and/or physically attached ferrocene/ferrocenium redox couple to polypyrrole, which is electrochemically active as Li-ion battery cathode materials, to promote its capacity and alleviate the ohmic/concentration polarization.[114] Astruc and co-workers demonstrated dendritic molecular electrochromic batteries based on redox-robust metallocenes.[115]

One of the most appealing characteristics of ferrocene as active material for Li-redox flow battery is the prompt redox kinetics.[116] The activation energy required for the two orbital electronic structure conversion is low ($\sim$10 kJ mol^{-1}) in most organic solvents with high rate constant (10^{-2}–10^{-3} cm s^{-1}),[117,118] which is orders of magnitude greater than those of the redox couples used in conventional redox-flow batteries. These properties together with good thermal stability and solubility promise ferrocene a potential material for Li-ion redox flow battery capable of providing maximized energy density and power density. It's found that the rate variations for ferrocenium/ferrocene redox reaction was only affected moderately by the electrolyte concentration and the presence of substituents on the Cp rings.[119–121] Nevertheless, the redox potential and redox reaction reversibility exhibit more obvious solvent-dependence possibly *via* interactions between the hydrogen-bonding acid and base moieties of the solvent and the members of the ferrocene/ferrocenium.[109]

Table 3 Redox behaviours of certain metallocenes

Compounds	Redox reaction	Redox potential	Supporting electrolyte	Reversibility
Titanocene dichloride	$TiCp_2^{2+} + e^- \leftrightarrow TiCp_2^+$	−0.80 V *vs.* Ag^+/Ag	0.1 M Bu_4NPF_6 in acetonitrile	Quasi-reversible
Vanadocene	$VCp_2^+ + e^- \leftrightarrow VCp_2$	*ca.* −0.7 V *vs.* Pt electrode	0.3 M Bu_4NPF_6 in THF	Reversible
Chromocene	$CrCp_2 + e^- \leftrightarrow CrCp_2^-$	*ca.* −2.3 V *vs.* Pt electrode	0.3 M Bu_4NPF_6 in THF	Reversible
	$CrCp_2^+ + e^- \leftrightarrow CrCp_2$	*ca.* −0.53 V *vs.* Pt electrode		Reversible
Decamethylmanganocene	$MnCp^*_2 + e^- \leftrightarrow MnCp^*_2{}^-$	−2.5 V *vs.* SCE	Bu_4NBF_4 in acetonitrile	Reversible
	$MnCp^*_2{}^+ + e^- \leftrightarrow MnCp^*_2$	−0.56 V *vs.* SCE		Reversible
Ferrocene	$FeCp_2^+ + e^- \leftrightarrow FeCp_2$	0.505 V *vs.* Ag^+/Ag	0.1 M Bu_4NClO_4 in acetonitrile	Reversible
Cobaltocene	$CoCp_2 + e^- \leftrightarrow CoCp_2^-$	−1.88 V *vs.* SCE	0.3 M Bu_4NPF_6 in acetonitrile	Reversible
	$CoCp_2^+ + e^- \leftrightarrow CoCp_2$	−0.94 V *vs.* SCE		Reversible
Nickelocene	$NiCp_2^+ + e^- \leftrightarrow NiCp_2$	−0.50 V *vs.* $FeCp_2^{+/0}$	0.05 M Bu_4NBF_4 in acetonitrile	Reversible
	$NiCp_2^{2+} + e^- \leftrightarrow NiCp_2^+$	0.49 V *vs.* $FeCp_2^{+/0}$		Reversible
Rhodocene	$RhCp_2^+ + e^- \leftrightarrow RhCp_2$	−1.41 V *vs.* SCE	0.1 M Bu_4NPF_6 in acetonitrile	Reversible
	$RhCp_2 + e^- \leftrightarrow RhCp_2^-$	−2.18 V *vs.* SCE		Quasi-reversible

Yu and co-workers investigated the solvent-dependent redox behaviour of ferrocene/ferrocenium redox couple, and found that the ferrocenium could be reduced at a high potential $\sim$3.6 V *vs.* Li^+/Li in $LiPF_6$/DMF supporting electrolyte with good reversibility and small polarization.[104] In comparison, the ferrocenium/ferrocene redox couple showed lower redox potential or higher polarization in other supporting electrolyte such as DMA, THF and EC/DEC organic electrolyte. The kinetic rate constant in DMF was determined to be 1.4×10^{-2} cm s^{-1} for ferrocene oxidation reaction and 6.8×10^{-3} cm s^{-1} for ferrocenium reduction reaction, both of which are considerably high compared to those of redox couples used in conventional aqueous or non-aqueous redox-flow batteries.[15] Owing to the rapid redox kinetics, the power density of this cell at room temperature reached 155 W kg^{-1} based on the total weight of the catholyte while maintaining a discharge potential of 2.4 V (Fig. 12a). The capacity retention was rather stable, and approximately 90% of the theoretical capacity could be maintained after 250 fully charge/discharge cycles (Fig. 12b).

Another important characteristic of ferrocene is the possibility to further tune the physical/chemical properties of ferrocene molecule, such as redox potential and solubility by means of functionalization with different function groups on the Cp ring through many well-established electrophilic reactions (Fig. 13). Formylation and carboxylation reactions give only monofunctionalization, because the functional group strongly deactivates the ferrocenyl group. On the other hand, metallation and acylation reactions can be followed by an identical reaction on the other ring leading to 1,1′-disubstituted derivatives, because the deactivation of the second Cp ring by the substituent is only modest.[105]

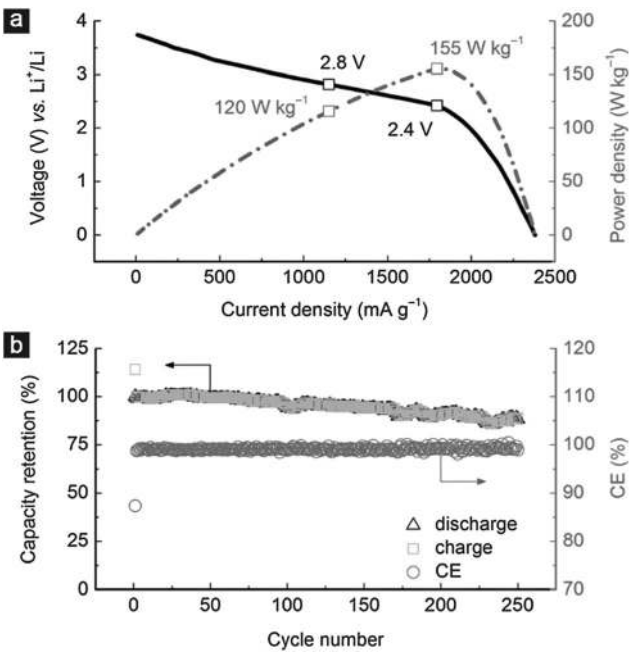

Fig. 12 Rate capability and cyclability of the Li-redox cell using ferrocene/ferrocenium redox couple. (a) Room temperature polarization curve. (b) Capacity retention with corresponding Coulombic efficiency over cycling. Reproduced with permission from ref. 104. Copyright 2014, Wiley.

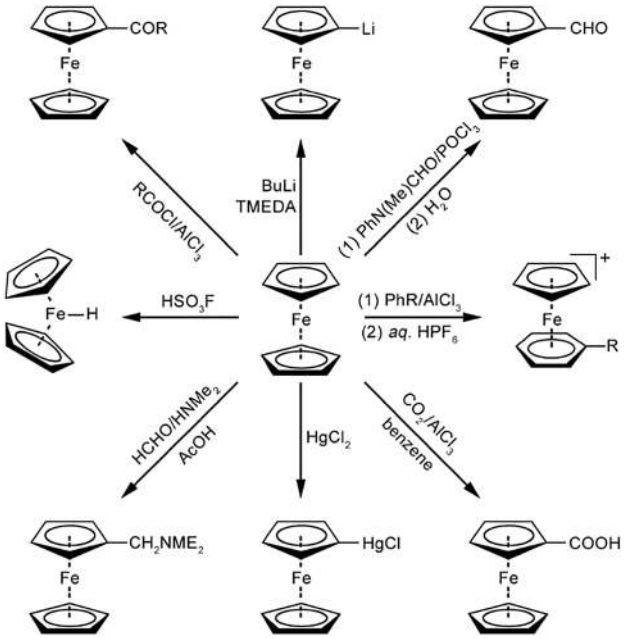

Fig. 13 Representative strategies to functionalize the ferrocene molecule with different function groups. Note that the as-obtained ferrocene derivatives can be used as precursors for further functionalization.

The redox potential of ferrocene derivatives were found to vary in a relatively broad range, from *ca.* +0.5 V when functionalizing pristine ferrocene with acetyl group on both Cp rings to *ca.* −0.5 V when the hydrogen atoms were substituted by methyl group.[122] Chemically modified ferrocene molecules with short carbon–carbon tethering arm composed of ethyl, vinyl and ethynyl groups showed difference in redox potentials about 0.2 V, following the increasing trend of the extent of unsaturation in the tethering arm.[123]

Wang and co-workers demonstrated a semi-solid Li-redox flow cell using $LiFePO_4$ nanoparticles as the Li^+-storage material, and binary ferrocene and its derivative as the mediator for redox targeting of the $LiFePO_4$ nanoparticles.[124] The general principle of the redox targeting method (Fig. 14a) is based on the chemical lithiation/delithiation of electro-active materials with poor electronic conductivity, which allows fast charge transport thus may enhance the power density of the cell.[125] They used 1,10-dibromoferrocene and ferrocene as the redox mediators, of which the half-wave potentials are 3.55 and 3.25 V *vs.* Li^+/Li, respectively (Fig. 14b). They demonstrated a similar cell using bis(pentamethylcyclopentadienyl)cobalt and cobaltocene as the redox mediator, and anatase TiO_2 as Li^+-storage material.[126] Such ''semi-solid'' electrode configuration might overcome solubility issue of the redox-active species. To alleviate the solid particle aggregation and promote the diffusivity of the redox mediators in concentrated viscose catholyte suspension, the deleterious effects of solid-electrolyte interface formation on electron transport, and system stability after long-term operation still remain challenging.

Proper functionalization may also improve the solubility of ferrocene. Wang and co-workers used functionalized ferrocene

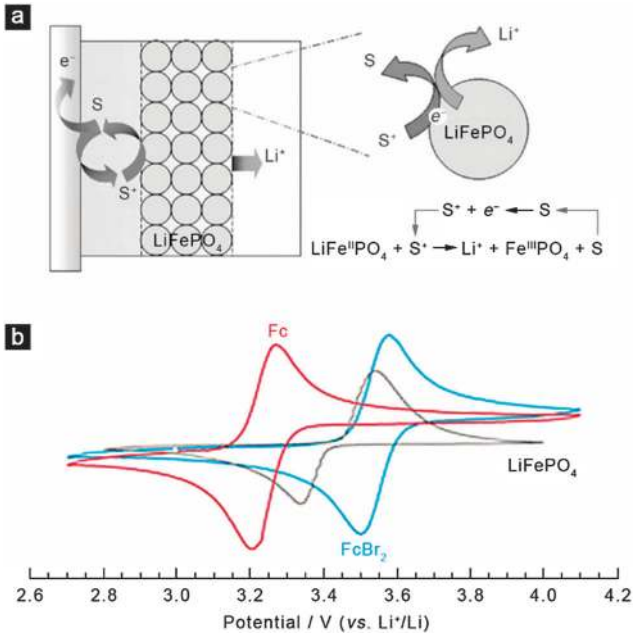

Fig. 14 (a) The principle of redox targeting of an insulating electrode material such as $LiFePO_4$ by a freely diffusing molecular shuttle S. Upon charging, the molecular shuttle is oxidized into S^+ at the current collector, and delivers the charge to the solid particles $LiFePO_4$. S^+ will be reduced back to S if the redox potential matches the Fermi level of $LiFePO_4$. During this process, Fe^{II} is oxidized into Fe^{III}, and Li^+ ions will be released. Upon discharge, S^+ is reduced at the current collector to S so electrons can be delivered to $FePO_4$ to form $LiFePO_4$ with the simultaneous immigration of Li^+ ions. Reproduced with permission from ref. 125. Copyright 2006, Wiley. (b) Cyclic voltammograms of the redox shuttles Fc and $FcBr_2$, as well as a cathodic Li^+-storage material $LiFePO_4$. Reproduced with permission from ref. 124. Copyright 2013, Royal Society of Chemistry.

molecule with an ionic charged tetraalkylammonium pendant arm and a $TFSI^-$ counter anion to serve as the active material for Li-redox flow cell application.[127] Through the density functional theory calculation, they found that the preferential sites for the solvent molecules were near and around the ionic region due to its higher positive charge density around the functionalized ferrocene cation. The ionic pendant intensifies the interactions between the solvent molecules and the functionalized ferrocene, resulting in a greatly enhanced solubility up to 0.85 M in the electrolyte of 1.2 M LiTFSI in EC/PC/EMC. The volumetric energy density thus reached $\sim$50 W h L^{-1} with good cyclability and energy efficiency.

As another type of metallocene analogue, cyclopentadienyl–metal–arene complexes show the advantage of robustness, the same type of redox properties, offering new possibilities to develop redox-active materials for Li-redox flow cells but yet to be demonstrated. For example, the redox couple of $[(\eta^5\text{-}C_5H_5)Fe(\eta^6\text{-}C_6Me_6)_2]^{+/0}$ show redox potentials of -2 V *vs.* $FeCp_2^{+/0}$ in THF,[128] which might be used as anolyte for Li-redox flow cell to yield a cell voltage around 2 V if configured with $FeCp_2^{+/0}$ catholyte. The redox couple of $[(\eta^5\text{-}C_5Me_5)Fe(\eta^6\text{-}C_6Me_6)_2]^{+/0}$ has a redox potential of -1.85 V *vs.* SCE that is independent on the nature of the solvent and electrolytes. $[(\eta^5\text{-}C_5Me_5)Fe^{III}(\eta^6\text{-}C_6Me_6)_2]^{2+}$ is an excellent oxidant that can be reversibly converted to $[(\eta^5\text{-}C_5Me_5)Fe^{II}(\eta^6\text{-}C_6Me_6)_2]^{+}$ at a high potential of $\sim$1 V *vs.* $FeCp_2^{+/0}$.[105] These complexes together with metallocenes and their derivatives can be regarded as an important new class of materials for Li-redox flow batteries. Nevertheless, the general rules for rational design and functionalization of targeted molecules with preferred characteristics need to be addressed before the technology could compete with current aqueous redox flow batteries, especially on the solubility and redox behaviour in concentrated solutions and that will eventually make a further step towards the practical application for the future electric grid.

4.2 Polysulphide-based Li-redox flow batteries

The Li–S battery system received considerable research interest in the past decades owing to its high gravimetric capacity and low cost and high abundance of elemental sulphur. In practice, the cell performance is plagued by poor cyclability mainly arising from the low ionic and electronic conductivity of sulphur, the sluggish reaction kinetics, large volume change during phase transformation between S and Li_2S_2/Li_2S, and the formation of soluble polysulphides,[129–132] among which $>$10 M S as $\sim Li_2S_9$ can be dissolved by the reaction of Li_2S and S_8.[133] The polysulphide-based catholyte instead of the solid sulphur-based electrode is an alternative choice to alleviate these problems. The catholyte can also enhance the reaction kinetics of electrode because of fast ion diffusion in liquid, and can be circulated in a flow system, showing promise as large-scale storage system.

The charge/discharge of Li–sulphur battery is a complex multistep process. XANES detects Li_2S formation near the middle of the second plateau, and this formation increases at the end of discharge.[134] Whereas, *in situ* synchrotron-based techniques indicate the formation of crystalline Li_2S on the positive electrode at the very beginning of the lower discharge.[135] *In situ* NMR spectroscopy study also suggested that sulphur is reduced to soluble polysulfide species during the first discharge plateau concurrently with the formation of Li_2S.[136] *In situ* XRD and transmission X-ray microscopy study suggests that crystalline Li_2S is not formed at the end of discharge and most of the intermediate polysulfides are retained inside the cathode matrix.[137] While experimental result shows that the lithiation/delithiation for S_{2-4} occurs as a solid–solid process if the micropores of carbon are small enough to prevent the penetration of the solvent molecules.[138]

Direct evidence for these proposed mechanisms is difficult to obtain due to multistep reactions that are further complicated by the formation of a variety of transient species. A plausible explanation indicated that the sulphur reduction consisting of three steps:[139] long polysulphide chains such as S_8^{2-} and S_6^{2-} are produced during the first reduction step (2.4–2.2 V *vs.* Li^+/Li),; S_4^{2-} is produced during the second reduction step (2.15–2.1 V *vs.* Li^+/Li); finally, short polysulphide species such as S_3^{2-}, S_2^{2-}, and S^{2-} are produced at the end of the reduction process (2.1–1.9 V *vs.* Li^+/Li). Very recently, Lu and co-workers employed the rotating-ring disk electrode technique and a lithium ion conducting solid electrolyte for elimination of the loss of active material to probe the reaction kinetics and reaction mechanism of lithium–sulphur redox reactions in DMSO and DOL/DME electrolytes.[140] They proposed that the electrochemical steps of sulphur reduction

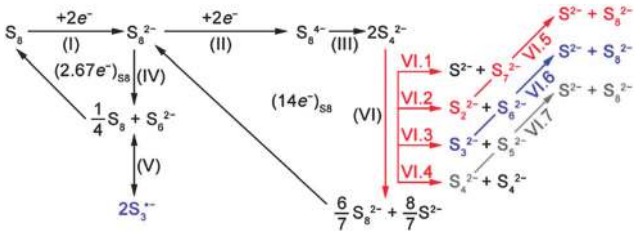

Fig. 15 Proposed sulphur reduction mechanism in liquid phase. The elemental sulphur is first reduced to S_8^{2-} *via* reaction (I), followed by the formation of S_8^{4-} *via* reaction (II). A subsequent dissociation of S_8^{4-} *via* reaction (III) leads to the formation of S_4^{2-}, or a disproportionation reaction *via* reaction (IV) to form S_8 and S_6^{2-}; the latter may dissociate to $S_3^{\bullet-}$ through reaction (V). An overall $2.67e^-/S_8$ process is established through reactions (I) and (IV). Reactions (I), (II), and (III) occur in both DMSO and DOL/DME, while reactions (IV) and (V) occur only in DMSO. The formed S_4^{2-} undergoes various subsequent chain-growth and disproportionation reactions to generate reducible species such as S_8^{2-} *via* reactions (VI.1)–(VI.4). Reactions (II), (III) and (VI) lead to a total $14e^-/S_8$ process. Reproduced with permission from ref. 140. Copyright 2014, American Chemical Society.

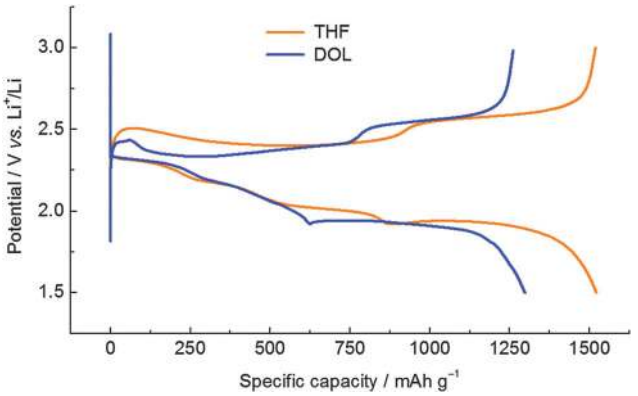

Fig. 16 Stabilized charge/discharge behaviour of polysulfide catholyte in DOL and THF. The catholyte is isolated from the Li anode in a cylinder cell by a NASICON-type $Li_{1+x+3z}Al_x(Ti,Ge)_{2-x}Si_{3z}P_{3-z}O_{12}$ glass ceramic. Carbon black/PVDF composite casted on Ti foil is used as current collector, and 0.5 M LiTFSI is used as lithium salt. The current rate is 0.1 C.

in liquid phase exhibited fast reaction kinetics and only accounted for approximately one-quarter of the total capacity within the short reaction time. The complete conversion of sulphur to Li_2S could only be accomplished *via* chemical polysulfide recombination/dissociation reactions that generated electrochemically reducible polysulfides with long reaction time in a closed cell (Fig. 15).

The first polysulphide Li-redox cell was proposed by Rauh and co-workers.[141] They used metallic Li as anode, polysulphide dissolved in THF/$LiAsF_6$ as the catholyte, and Teflon bonded carbon as current collector. The cell achieved a high utilization of 1.83 Li^+ per sulphur in the initial discharge owing to the high reactivity of soluble polysulfides compared to solid sulphur particles. The efficiency of the cell reached 90% with discharge depth of 0.5 Li^+ per sulphur at 50 °C, but deteriorated quickly after 10–20 cycles, which probably raised from the lack of the lack of effective protection method to block the shuttle effect between soluble polysulfides and Li.

To make practical polysulphide-based Li-redox flow cells, one strategy is to passivate the Li anode to inhibit the electron hopping to polysulfide anions. Zhang and co-workers used $LiNO_3$ to promote Li anode passivation and improve the cycling performance with a good capacity retention over 70 cycles.[142] Their electrochemical analyses on Li_2S_9 catholyte with $LiNO_3$ additive revealed the formation of a highly resistive passivation film on the Li metal surface, thus effectively alleviated the shuttle effect. Cui and co-workers adopted a similar $LiNO_3$-passivated Li-anode to construct a membrane-free Li-redox cell.[103] In contrast to aforementioned polysulphide-based Li-redox cells, the catholyte is designed to cycle only between Li_2S_8 and Li_2S_4 by narrowing the potential window to 2.15–2.8 V. Despite the theoretical capacity limit being restricted to 418 mA g^{-1}, the cell could still reach an energy density of 97 W h kg^{-1} or 108 W h L^{-1}, owing to the high solubility of Li_2S_x ($4 \leq x \leq 8$).

Another strategy is to optimize the composition of electrolytes. Conventional carbonate-based electrolytes may not be as promising as in Li-ion batteries, because the polysulfides can react with carbonate-based electrolyte *via* nucleophilic addition or substitution to form thiocarbonates and other small molecules.[143,144] The charge/discharge behaviour of polysulfide catholyte is very sensitive to the polarity of the supporting electrolyte. The poor stabilization of polysulfides in low-dielectric solvents such as THF and DOL seems beneficial to achieve high reversible capacity (Fig. 16). In general, solvents with high dielectric constant such as amides, sulfoxides, nitriles *etc.* exhibit stronger ability to stabilize charged species compared to solvents with low dielectric constant such as ethers, furans, amines, ionic liquids, *etc.*[145] Rauh and co-workers showed that polysulphide intermediate is not formed in imidazolium ionic liquid during extended bulk electrolysis, but clear $S_3^{\bullet-}$ formation observed in DMSO.[146] Tobishima and co-workers suggest that the stability of polysulfide intermediates increases with the dielectric constant of the solvents.[147] Lu and co-workers show that only part of the sulphur reduction capacity is obtained through direct electrochemical steps, and that the rest of the capacity is achieved *via* subsequent chain-growth and disproportionation reactions.[140]

An additional strategy is to improve the cell design such as choosing proper separator membrane and designing effective electrode architecture, which could prevent the polysulphides from emigrating to the anode side and provide conductive matrices to promote the redox kinetics of polysulphides.[148–151] Polymeric and glass-ceramic separator membranes are more effective than liquid electrolytes to block the shuttle effect and dissolution of polysulfides in solid-state Li–S batteries as well as alleviate the dendrite formation on Li anode. The practicability for polysulphide catholyte needs further investigation. Polymeric membranes are easily penetrated by polysulphides and solvent molecules owing to the large gap between the polymer chains. Glass-ceramic membranes such as thio-LISICONs[152,153] and Li_2S–P_2S_5 glasses[154,155] are yet to be demonstrated in the polysulphide-based Li-redox flow cell. The NASICON-type $Li_{1+x+3z}Al_x(Ti,Ge)_{2-x}Si_{3z}P_{3-z}O_{12}$ glass ceramic seems promising to polysulphide catholyte (Fig. 16).

Rationally designed electrode architecture would help improve the performance of the polysulphide catholyte. Electrodes made

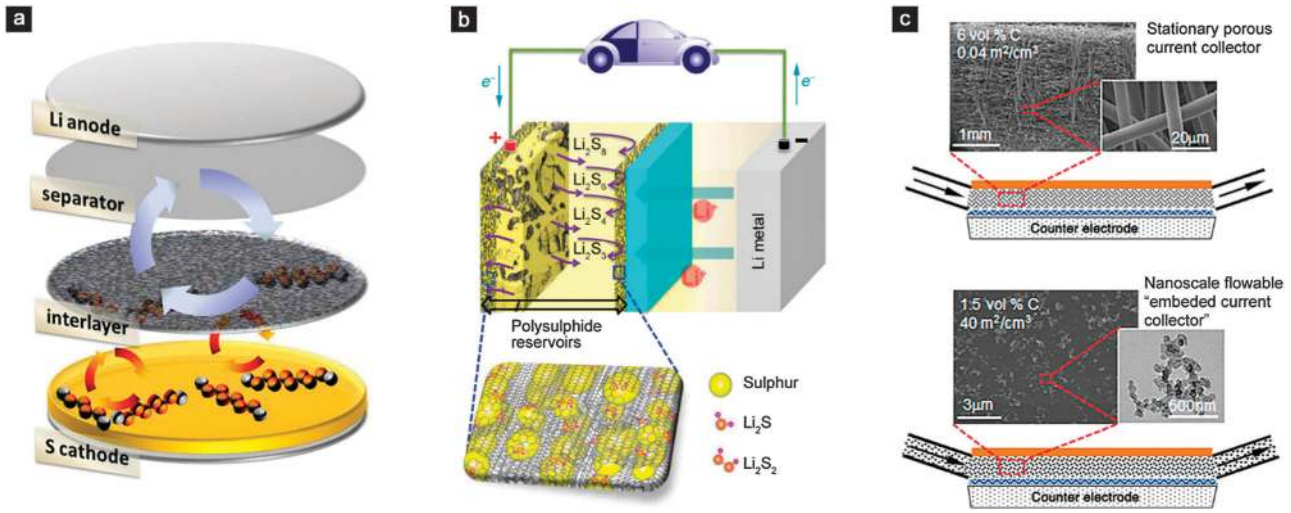

Fig. 17 Electrode architectures for polysulphide-based Li-redox flow cells. (a) Bi-functional interlayer electrode architecture. Reproduced with permission from ref. 150. Copyright 2014, American Chemical Society. (b) Compound-sandwiched electrode architecture. Reproduced with permission from ref. 167. Copyright 2014, Wiley. (c) Conventional flow cell architecture using stationary carbon fibre current collector (top) and nanoscale flowable "embedded current collector" (bottom) providing electronically conductive flowing redox electrodes based on nanoscale percolating networks of carbon black particles. Reproduced with permission from ref. 168. Copyright 2014, American Chemical Society.

from conductive porous materials have been investigated and turned out to be promising.[156–161] Porous current collector architectures as polysulfide reservoir show the capability for efficient conversion among the polysulfide species,[156,162,163] but the diffusion of polysulphides cannot be totally inhibited. Introducing a bi-functional interlayer (Fig. 17a) between the separator and the current collector as a polysulfide-diffusion inhibitor seems a plausible strategy to promote the cyclability of the polysulfides.[164,165] Manthiram and co-workers proposed a compound-sandwiched electrode architecture that includes a bi-functional interlayer on the top, the active material in the middle, and a porous current collector at the bottom.[166] Such a cell configuration showed good electrochemical performance both in polysulfide catholyte and regular sulphur cathode. Cheng and co-workers demonstrated a high-performance solid-state lithium–sulphur batteries by using the compound-sandwiched electrode architecture consisting of a sulphur electrode in between a porous graphene free-standing film and a commercial polymer separator that is coated with another porous graphene free-standing film (Fig. 17b).[167] The cyclability of the cell was greatly enhanced due to the electrode architecture that served as effective polysulfide reservoir to localize the dissolved polysulfides. However, these electrode configurations can only partially localize the migrating polysulfides within the cathode region. Though the formation of insoluble species would not seriously affect the performance of a static cell, these insoluble species may not reversibly convert to polysulphides when away from the electrode region in a flow cell configuration. Chiang and co-workers proposed a nanoscale flowable "embedded current collector" (Fig. 17c) applicable to redox flow chemistries which undergo precipitation–dissolution reactions.[168] In their design, the percolating networks of conductive carbon were incorporated within fluid electrodes, allowing the polysulfide catholyte to be reversibly cycled into composition regimes where Li_2S precipitation occurs. Very recently, Zhou and co-workers report a prototype of a solar-driven chargeable lithium–sulphur battery, in which the capture and storage of solar energy was realized by oxidizing S_2^- ions to polysulfide ions in aqueous solution with a Pt-modified CdS photocatalyst.[169] Such a device realized simultaneous electrochemical energy storage and hydrogen production by introducing a photocatalyst into a lithium–sulphur battery, thus providing a new thread towards direct conversion between chemical energy and solar energy.

4.3 Organic-based Li-redox flow batteries

Depending on the reduction of the neutral state, organic redox molecules can be generally categorized into three types (Fig. 18a):[170] n-type organics, of which the redox reaction is between the neutral state and the negatively charged state;[171] p-type organics, of which the redox reaction is between the neutral state and the positively charged state;[172] and bipolar organics, of which the neutral state can be either reduced to a negatively charged state or oxidized to a positively charged state.[173,174] In the electrochemical reduction reaction of n-type organics or oxidation reaction of p-type organics, the corresponding cations (*e.g.* Li^+ or Na^+) or anions (*e.g.* PF_6^-, ClO_4^- or $TFSI^-$) are needed to neutralize the charge. In the reverse redox process, cations or anions will migrate back from the electrode to the electrolyte. For many n-type organics, Li^+ can be substituted by other alkali metals, which will not affect significantly their redox behaviour in general. In principle, these redox-active organic molecules could be also used in Li-redox cells with advantages such as overcoming the dissolution problem of small organic molecules in conventional rechargeable solid batteries, and increasing the solubility by adding proper function groups or using proper non-aqueous electrolyte.

For n-type redox-active organics, considerable research interest has been focused on carbonyl compounds. Carbonyl is a common organic functional group that shows oxidative ability.

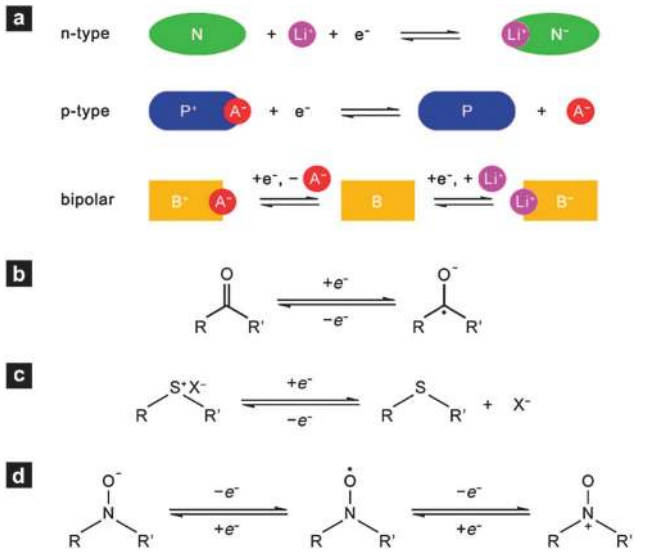

Fig. 18 (a) Redox reaction of n-type (N), p-type (P) and bipolar (B) redox-active organics and metallorganics. A^- stands for anion of the electrolyte. Reproduced with permission from ref. 170. Copyright 2013, Royal Society of Chemistry. Corresponding redox mechanism for redox-active organics: (b) carbonyl compounds, (c) thioethers, and (d) organic free radical compounds.

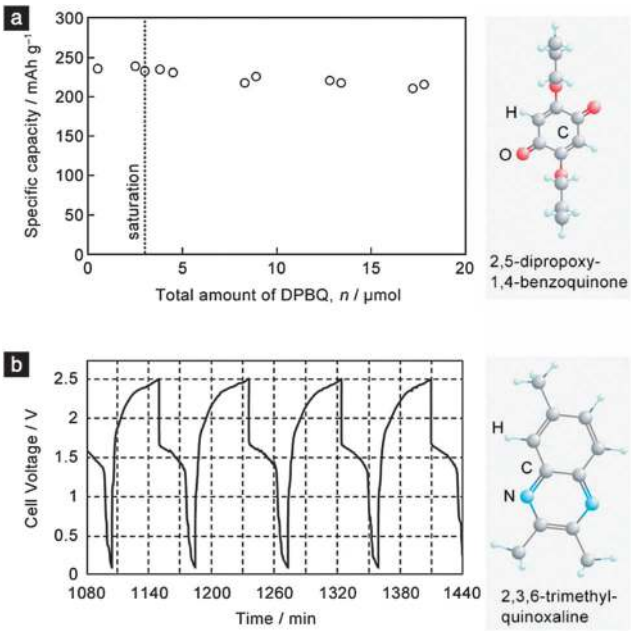

Fig. 19 Representative examples of n-type redox-active organics for Li-redox flow cell. (a) Relation between the total amount of 2,5-dipropoxy-1,4-benzoquinone (DPBQ, molecular structure shown on the right) in the catholyte and capacity in the 10th discharge. The dotted line indicates the solubility of DPBQ. Reproduced with permission from ref. 177. Copyright 2011, Elsevier. (b) Charge/discharge profiles of the all-organic Li-redox flow cell using 0.05 M 2,5-di-*tert*-butyl-1,4-bis(2-methoxyethoxy)benzene and 0.05 M 2,3,6-trimethylquinoxaline (molecular structure shown on the right) as the high- and low-potential active species. Reproduced with permission from ref. 19. Copyright 2012, Wiley.

In presence of appropriate stabilizing groups, the carbonyl group undergoes reversible one-electron reduction to form a radical monoanion (Fig. 18b). The redox centre of conjugated carboxylates locates in the weakly electron-withdrawing carboxyl groups, and the redox process involves the resonance of conjugated bonds in the carbon chain and regrouping the electrons into a set of conjugated bonds.

Tarascon and co-workers demonstrated that Li terephthalate and Li *trans–trans*-muconate were respectively capable of reacting with two and one extra Li per formula unit at potentials of 0.8 and 1.4 V *vs.* Li^+/Li.[175] They also demonstrated that 4,4′-tolane-dicarboxylate could also be used as a negative electrode material in Li^+-ion batteries with discharge potential of 0.65 V *vs.* Li^+/Li and minimal discharge/charge polarization.[176] The solubility of lithium salts of these highly conjugated molecules is usually low if directly used as anode materials in Li-redox flow cells. Quinones and their derivatives show good solubility in certain aprotic electrolytes. The discharge process of quinones and their derivatives is driven by two-electron disproportionation: the formation of a radical anion in the first stage followed by dianion formation in the second stage. Siroma and co-workers examined the electrochemical performance of 1,4-benzoquinone and its derivatives in a Li-redox cell, and showed that the cyclability was inversely proportional to its concentration in the catholyte[177] They suggested that sublimation of 1,4-benzoquinone, instability of the radical anion, low reactivity of reduction products were responsible for the concentration-dependent cyclability. They also suggested that to introduce peripheral substituents into the 1,4-benzoquinone moiety might suppress sublimation and stabilize the intermediate radical species, which was successful in their subsequent attempts by using 2,5-dipropoxy-1,4-benzoquinone (Fig. 19a). Wang and co-workers used a modified anthraquinone, 1,5-bis(2-(2-(2-methoxy-ethoxy)ethoxy)ethoxy)anthracene-9,10-dione, with improved solubility to the anthraquinone counterpart to serve as the energy bearing redox active agent.[178] The introduction of two triethylene glycol monomethyl ether groups into the anthraquinone molecular structure had a large effect on the solubility, and the resulting molecule was soluble in most polar solvents and aprotic electrolytes. Jansen and co-workers reported an organic Li-redox flow cell using 2,3,6-trimethylquinoxaline as anode-active material and 2,5-di-*tert*-butyl-1,4-bis(2-methoxyethoxy)benzene as cathode-active material.[19] The cell charged and discharged from 1.8–2.4 V and 1.7–1.3 V, respectively, after an initial acclimatization period (Fig. 19b). The cell showed a relatively low Coulombic efficiency of ~70% and an energy density of ~12 W h L^{-1}, which revealed one of the major difficulties by using n-type redox-active organics in increasing the solubility while harvesting the full potential of this design.

Till now, redox-active p-type organics have not yet been explored for Li-redox flow batteries. Perspective candidates are organosulfur compounds, such as thioethers, thioesters, sulfuranes, and anthracene or naphthalene derivatives bearing dithiol ring and/or methylsulfide. For instance, thioethers undergo reversible electron-extraction to form stable cationic radical species (Fig. 18c), and the reversible redox reaction at room temperature *via* one-electron oxidation per sulphur is kinetically fast.

For bipolar redox-active organics, nitroxide-based polymers are the most studied radical compounds for electrode application.[179] While many organic molecules experience a significant

structural rearrangement upon oxidation, nitroxides benefit from the localization of the electron density at the N–O centre and only slight structural changes.[180] Chemical stability of both the radical and the doped forms is essential for durability of the charging and discharging processes of the battery. Besides, the electron-transfer rate constant for the nitroxide radicals in solution is estimated to be on the order of 10^{-1} cm s^{-1},[181] which is the most important feature when compared to the slow rates for other organic redox reactions. One of the best known stable nitroxide is TEMPO (2,2,6,6-tetramethyl piperidine-1-oxyl). Theoretical investigation suggests that TEMPO and its certain derivatives can be reversibly n-doped to aminoxy anion and p-doped to oxoammonium cation in cathodic and anodic reactions, respectively (Fig. 18d).[182] In aprotic phase, the TEMPO and TEMPO-base radicals usually show reversible redox reaction between the neutral state and oxidized state with redox potential in the range of 3.4–3.9 V *vs.* Li^+/Li.[183] Other stable radicals (shown in Fig. 20) with proper redox potentials may be worthy investigating but yet to be developed in Li-redox flow cells, such as spirobisnitroxide (~0.8 V *vs.* Ag^+/Ag),[184] arylnitroxide (*ca.* 0.7 V *vs.* Ag^+/Ag),[185] arynitroxide (*ca.* −0.7 V *vs.* Ag^+/Ag),[185] nitronylnitroxyl (*ca.* 0.7 V *vs.* Ag^+/Ag upon oxidation, *ca.* −0.6 V *vs.* Ag^+/Ag upon reduction),[186] galvinoxyl (*ca.* 0.06 V *vs.* Ag^+/Ag),[172] and PROXYL (2,2,5,5-tetramethyl-2,5-dihydro-1*H*-pyrrol-1-oxyl-3-yl, *ca.* 0.5 V *vs.* Ag^+/Ag)[187] *etc*.

The first demonstration using TEMPO radical as cathode-active materials for non-aqueous redox flow battery was achieved by Liu and co-workers.[188] The cell was constructed from a TEMPO/$NaClO_4$/acetonitrile catholyte, *N*-methylphthalimide/$NaClO_4$/acetonitrile anolyte, and a Nepem-117 cation-exchange membrane as the separator with Na^+ as the charge carrier. TEMPO and *N*-methylphthalimide showed a redox potential around 0.4 V and −1.3 V *vs.* Ag^+/Ag, respectively (Fig. 21a). The cell showed a discharge potential of 1.4 V with 0.3 V overpotential during charge, and the Coulombic efficiency reached 90% for the demonstrated 20 cycles. Wang and co-workers further verified the reversibility of TEMPO radical.[189] They found that TEMPO concentration exhibited a linear relationship with the charge time revealed by electron spin resonance (ESR) spectroscopy (Fig. 21b), indicating that the redox reaction between TEMPO free radical and

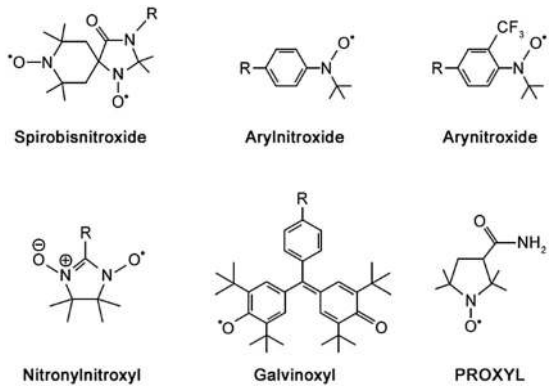

Fig. 20 Representative free radicals might be used in Li-redox flow batteries.

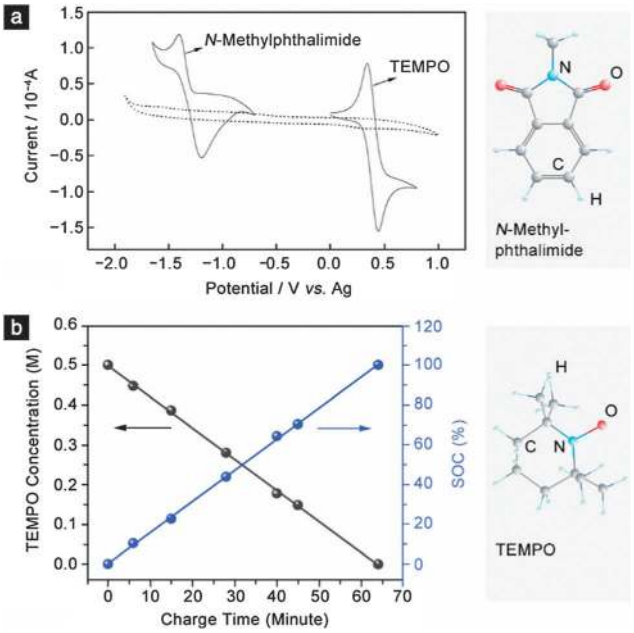

Fig. 21 (a) The Cyclic voltammograms of 0.02 M TEMPO/1.00 M $NaClO_4$/acetonitrile, 0.02 M *N*-methylphthalimide/1.00 M $NaClO_4$/acetonitrile and 1.00 M $NaClO_4$/acetonitrile (dotted line) under the scan rate of 10 mV s^{-1}. Reproduced with permission from ref. 188. Copyright 2011, The Electrochemical Society. (b) The ESR-measured TEMPO concentration and state-of-charge (SOC) of the flow cell with respect to the charge time. Reproduced with permission from ref. 189. Copyright 2012, Wiley.

oxoammonium cation was totally reversible in $LiPF_6$/EC–PC–EMC supporting electrolyte.

The energy density of present organic Li-redox batteries is far behind their inherent capability with the major bottleneck being the low solubility of electroactive materials. Meanwhile, metallic Li could be replaced by proper redox-active molecules with low redox potential for the better safety and total modular design of the cell. The use of electroactive organic species may offer the opportunities for the design and synthesis of novel organic molecules with tailorable redox potential, solubility, and electrochemical activity. Some redox-active organic compounds that, with proper modification to address the solubility issue, would show potential for Li/Na-redox cells are summarized in Fig. 22.[19,104,126,170,172,175,176,188–198]

5. Separator membranes for Li-redox flow batteries

The separator membrane is one of the most critical components in the Li-redox batteries. There are two general classes of materials used for separator membranes in Li-redox batteries depending on the cell configuration: inorganic ceramics (solid electrolyte) and organic polymers (polymeric electrolyte). The most obvious difference between these classes is the mechanical properties. The high elastic moduli of ceramics make them more suitable for rigid cell designs. Conversely, the low elastic moduli of polymers are useful for flexible cell designs.

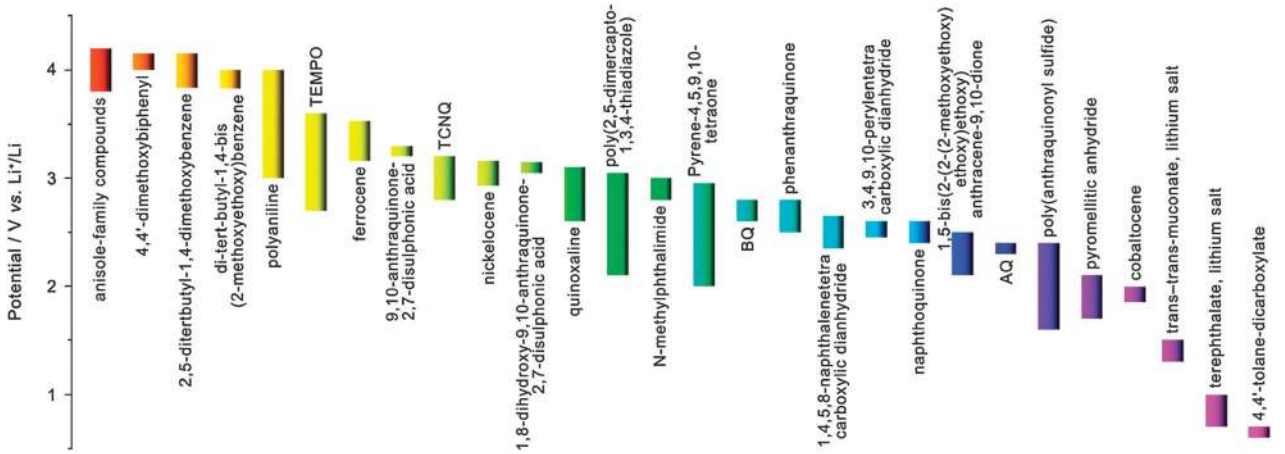

Fig. 22 Redox potential of representative redox-active organic and organometallic compounds with potential for organic-based Li/Na-redox cells.

Common requirements of the solid Li^+ electrolyte for battery applications includes: (i) a Li^+ conductivity $>10^{-4}$ S cm^{-1}, a low resistance to Li^+ transfer across its interfaces at the operating temperature, and no electronic conductivity, (ii) chemical stability in its working environment, (iii) containing only low-cost, non-toxic elements, and (iv) ease of fabrication into a mechanically robust, thin, and high-density membrane, especially for solid separators. Some characteristics such as stability and ionic conductivity of certain solid and polymeric electrolytes suitable for Li-redox flow battery application is summarized in Table 4. Here we review oxide Li^+ electrolytes and their stability on contact with metallic lithium and also with water and moist air. We conclude that the oxides containing mobile Li^+ will react with water unless the oxygen in the framework forms a strong covalent bond with a framework cation. Polymeric electrolytes are also briefly discussed.

5.1 NASICONs

The $B_2(XO_4)_3$ NASICON crystal structure consists of a $B_2(XO_4)_3$ three-dimensional rigid framework with BO_6 octahedra sharing corners with XO_4 tetrahedral (Fig. 23a);[199] the $B_2(XO_4)_3$ units may form a rhombohedral or an orthorhombic array; the rhombohedral phase provides better conduction pathways for a guest A^+ cation but realizing the rhombohedral phase is more difficult with a Li^+ guest ion than with a Na^+ guest. Moreover, the interstitial space of the rhombohedral framework contains one M^I to three M^{II} sites; the M^I site is occupied first, so an $x > 1$ is needed to obtain a fast A^+-cation conductivity. Presently, the best commercially available solid oxide Li^+ electrolyte is rhombohedral $Li_{1.3}Ti_{1.7}Al_{0.3}(PO_4)_3$ (LATP), with a Li^+ conductivity of (1–4) $\times$ 10^{-4} S cm^{-1} at 25 °C.[200,201] Substitution of a trivalent Al^{3+} or Sc^{3+} for some Ti^{4+} increases x of $A_xB_2(XO_4)_3$ and, therefore, also the Li^+ conductivity 10^{-6} S cm^{-1} at 25 °C of $LiTi_2(PO_4)_3$. To realize a commercial product, low-cost fabrication of a dense membrane is also needed. In addition, to the higher x or a higher bulk Li^+ conductivity, a higher density membrane increases Li^+ transport across the grain boundaries. Strong covalent bonding in the XO_4 units prevents attack by water. A high Li^+ conductivity in the bulk and across grain boundaries has also been obtained by sintering $LiTi_2(PO_4)_3$ with a lithium salt (Li_3BO_3, Li_3PO_4, and/or Li_2O);[202,203] the enhancement of Li^+ conductivity was attributed to a higher membrane density and Li^+-ion concentration in the grain boundaries. LATP glass with a Li^+ conductivity of 1.3 $\times$ 10^{-3} S cm^{-1} at 25 °C was shown to be unstable on contact with metallic lithium owing to Ti^{IV} reduction;[62,86] and on exposure to water, LATP can only be used in a limited pH range.[37] Therefore, NASICON-type $LiZr_2(PO_4)_3$ (LZP), has been explored as Zr^{IV} in an isolated octahedron can be expected to be chemically more stable than Ti^{IV}.[204,205] Substitution of Ca^{2+} or Y^{3+} for Zr^{4+} in LZP can stabilize the rhombohedral phase; it also increases the Li^+ conductivity to above 10^{-4} S cm^{-1} at 25 °C. The Li^+ conductivity of LZP may be improved by optimizing the doping element and its content and/or by increasing the density of the electrolyte membrane.

5.2 Garnets

The cubic $A_3B_3C_2O_{12}$ garnet structure consists of an $A_3C_2O_{12}$ framework with an interstitial space containing B_3 in tetrahedral sites that are bridged by empty octahedral sites sharing opposite faces with the tetrahedral sites (Fig. 23b).[206] This interstitial space is similar to that of the cubic M_2O_4 framework of the AM_2O_4 spinels. Fast Li^+ transport in the interstitial space of the spinel framework has been exploited for Li-insertion electrodes. Li-rich garnets have been studied extensively as Li^+ solid electrolytes since the observation of a Li^+ conductivity in exceed of 10^{-4} S cm^{-1} at 25 °C in $Li_7La_3Zr_2O_{12}$, which is stable on contact with a lithium anode.[207] Since Coulomb repulsions between Li^+-ions prevent occupancy of an octahedral site with its two near-neighbor tetrahedral sites occupied, x = 7.5 is the upper limit of x that can be tolerated in the $Li_xB_3C_2O_{12}$ garnet framework, and this limit requires the 1.5 vacancies per formula unit to be long-range ordered in the tetrahedral sites.[208] Therefore, substitution of Zr^{IV} by Ta^V or Nb^V has been used to increase the number of empty interstitial sites and to realize a Li^+ conductivity of 10^{-3} S cm^{-1} at 25 °C.[207,209] However, samples were commonly fired in an alumina boat, and incorporation of

Table 4 Summary of the stability and ionic conductivity of certain solid and polymeric electrolytes for Li-redox flow batteries

Electrolytes	Stability in water	Stability against Li/Na	Ion selectivity	Bulk conductivity (S cm^{-1}, at 25 °C)	Demonstrated conductivity (S cm^{-1}, at 25 °C)
NASICON-type LATP	Stable	Unstable	Li^+	1.3×10^{-3}	10^{-4}–10^{-3}
NASICON-type LZP	N/A	Stable	Li^+	2×10^{-4}	10^{-5}–10^{-4}
Garnet-type $Li_7La_3Zr_2O_{12}$	Unstable	Stable	Li^+	1×10^{-3}	10^{-4}–10^{-3}
Perovskite (Li,La)TiO_3	Unstable	Unstable	Li^+	1×10^{-3}	10^{-5}–10^{-3}
Perovskite (Li,Sr,Zr,Ta)TiO_3	Unstable	Unstable	Li^+	3.5×10^{-4}	10^{-5}–10^{-4}
Anti-perovskite Li_3OX	Unstable	Stable	Li^+	2×10^{-3}	10^{-6}–10^{-3}
Polymeric electrolyte	Stable	Stable	Li^+, Na^+	N/A	10^{-6}–10^{-4}

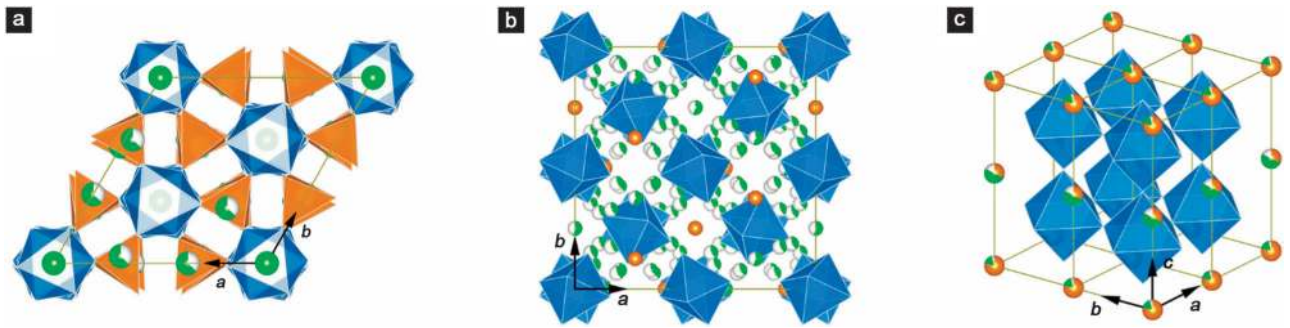

Fig. 23 Crystal structure of (a) NASICON-type $A_xB_2(PO_4)_3$, (b) Garnet-type $A_3B_3C_2O_{12}$, and (c) perovskite AMO_3.

adventitious Al^{3+} stabilized the cubic phase with $6 < x < 7$. Al_2O_3 was also used as a sintering aid to obtain ceramics with a high bulk Li^+ conductivity.[210,211] Control of the sintering conditions by using a dry O_2 atmosphere also leads to the formation of a dense ceramic and avoids degradation from the exchange of Li^+ by an H^+ of atmospheric moisture; a highest Li^+ conductivity of 1.2×10^{-3} S cm^{-1} at 25 °C has been reported.[212] Reaction with the H_2O of $Li_xB_3C_2O_{12}$ garnets having an $x > 3$ has prevented use of the garnet Li^+ solid electrolytes. With $x \leq 3$, the Li^+ occupy only the tetrahedral sites and the ceramic is stable in water, but Li^+ conductivity is low.[213] With $x > 3$, the octahedral-site Li^+ exchange with H^+ from water, and a strong hydrogen bond distorts the octahedral site.[214]

5.3 Perovskites and antiperovskites

The MO_3 framework of an AMO_3 perovskite (Fig. 23c), accepts Li^+ ions into the large empty A sites of an A-site-deficient perovskite. The $La_{2/3}M^{IV}O_3$ perovskite is an example, and $La_{3x}La_{2/3-x}\square_{1/3-2x}TiO_3$ ($0 < x < 0.16$) has been reported to have a bulk Li^+ conductivity $\sim 10^{-3}$ S cm^{-1} at 25 °C with $x \approx 0.1$.[215] The Li^+ are displaced off center of their large A-site cavity to either distorted tetrahedral sites or the square planar face of the MO_3 framework that does not face a La^{3+} ion. This electrolyte is unstable on contact with metallic lithium owing to Ti^{IV} reduction, and a large grain-boundary resistance to Li^+ conductivity at 25 °C lowers the conductivity to 10^{-5} S cm^{-1}. A $Li_{3/8}Sr_{7/8}Zr_{1/4}Ta_{3/4}O_3$ with a room-temperature Li^+ conductivity of 2×10^{-4} S cm^{-1} has been reported to have a better grain-boundary conductivity and a better stability against metallic Li,[216,217] but the sensitivity of these perovskites to water was not reported. A nominal Li_3OCl with the cubic antiperovskite structure with Li^+ conductivity $>10^{-3}$ S cm^{-1} at 25 °C with an activation energy of 0.2 to 0.3 eV has been reported.[218] However, the Li_3OX (X = Cl, Br, or I) antiperovskites are extremely hygroscopic; an H^+ of water exchanges for one Li^+ per formula unit.[219] Moreover, calculations have reported that an Li_3OX electrolyte could only be used in a low-voltage all-solid-state Li-ion battery.[220]

5.4 Polymeric electrolytes

Polymeric electrolyte, generally divided into solid and gel ones, have been extensively explored in lithium ion batteries because of their structural flexibility, excellent mechanical strength and improved operation safety. However, certain challenges still exist that obstruct the application of polymeric electrolytes in Li-redox flow batteries. The ionic conductivity of polymeric electrolytes is still low and should be improved to at least 10^{-4} S cm^{-1} at room temperature in order to meet the requirements of practical applications. Gel polymer electrolytes, having the characteristics of both solid and liquid electrolytes, provide a promising strategy towards satisfied ionic conductivity, wide electrochemical window, and good compatibility with electrodes. The favorable polymer matrixes for gel polymer electrolytes include PEO,[221] poly(acrylonitrile),[222] poly(methyl methacrylate),[223] PVDF,[224] and PVDF based copolymers, such as PVDF-*co*-trifluoroethylene and PVDF-*co*-hexafluoropropylene.[225,226] The typically micrometer-sized pores in these polymer matrixes ensure facile pathways of lithium ions, but lack the ability to prevent soluble redox species from crossing over the membrane. The concentration difference of anolyte and catholyte would induce osmosis that leads to the rapid fade of capacity and increased polarization. Polypropylene separator coated with a thin film of a conducting polymer, *i.e.*, PEDOT:PSS, has been proved efficient to prevent the crossover of redox-active ferrocene molecule from the catholyte to the anode. When coupled

with cross-linked PEO polymer electrolytes, the Li-redox flow cell exhibited stale cycle life without capacity fade after 50 charge/discharge cycles.[227]

The rate capability and life-span of the cell largely depend on the development of superior Li^+-ion conducting membranes. Currently, the thermal evolution of ionic conductivity of the solid electrolytes and polymeric solid electrolytes suitable for Li-redox flow battery application are summarized in Fig. 24.[25,58,95,228–243] Polymeric solid electrolytes combine the advantages of solid-state electrochemistry with the ease of processing inherent to plastic materials. However, it's necessary to overcome their relatively poor mechanical integrity and temperature endurance, which in turn might be enhanced by using polymers with supramolecular architectures,[244] and by using thermally stable polymer matrix and lithium salts.[245] The crystallinity of polymer should be suppressed and segmental motion should be maximized to achieve a sufficiently wide potential window and a Li^+ conductivity $>10^{-3}$ S cm^{-1} yet to be demonstrated.[246] Also, they should be able to block dendrites growth on Li anode or block soluble redox species in the cathode side from crossing over to the anode. Crystalline ionic conductors, in general, are advantageous over the polymeric solid electrolytes in terms of conductivity and stability. Material design of crystalline ionic conductors are based on certain structural criteria: mobile ions should have a suitable size for conduction pathways in the lattice, there should be disorder in a mobile ion sublattice, and highly polarizable mobile ions and anion sublattices are preferable. In general, oxide materials are believed to be superior to polymeric materials for reasons of handling and mechanical, chemical, and electrochemical stability.[229,236] These materials include perovskite oxides based on $(La,Li)TiO_3$, garnet oxides based on $Li_5La_3Ta_2O_{12}$,[215,247,248] crystalline sulfides such as Li_2S–P_2S_5 glass or glass-ceramic,[249–252] and phosphates similar to the Na^+-ion conducting NASICON compounds such as $Li_{1+x}Al_xGe_{2-x}(PO_4)_3$, $Li_{1+x}Ti_{2-x}Al_x(PO_4)_3$, and $Li_{1+x+y}Ti_{2-x}Al_xSi_y(PO_4)_{3-y}$.[232,253–256] All these materials exhibit bulk ionic conductivity of 10^{-3} S cm^{-1}. However, it is of utmost importance to decrease the grain-boundary resistivity of the oxide- or phosphate-based solid electrolytes. The instability of perovskite- and NASICON-type solid electrolytes against metallic Li and the solid/liquid interface need to be improved as well.[257–259] It's reported that using polymeric solid electrolyte as a buffer layer could alleviate the instability of NASICON-type solid electrolytes,[64,243,260–262] the long-term stability, however, needs further confirmation.[58] The development of solid electrolytes with superior conductivity and electrochemical stability will undoubtedly stimulate the development of Li-redox flow batteries together with a deep understanding of the fundamentals on ionic mobility in the bulk material.

6. Conclusion and future perspective

Li-redox flow batteries are still in their infancy, offering many exciting opportunities. The known redox couples and their

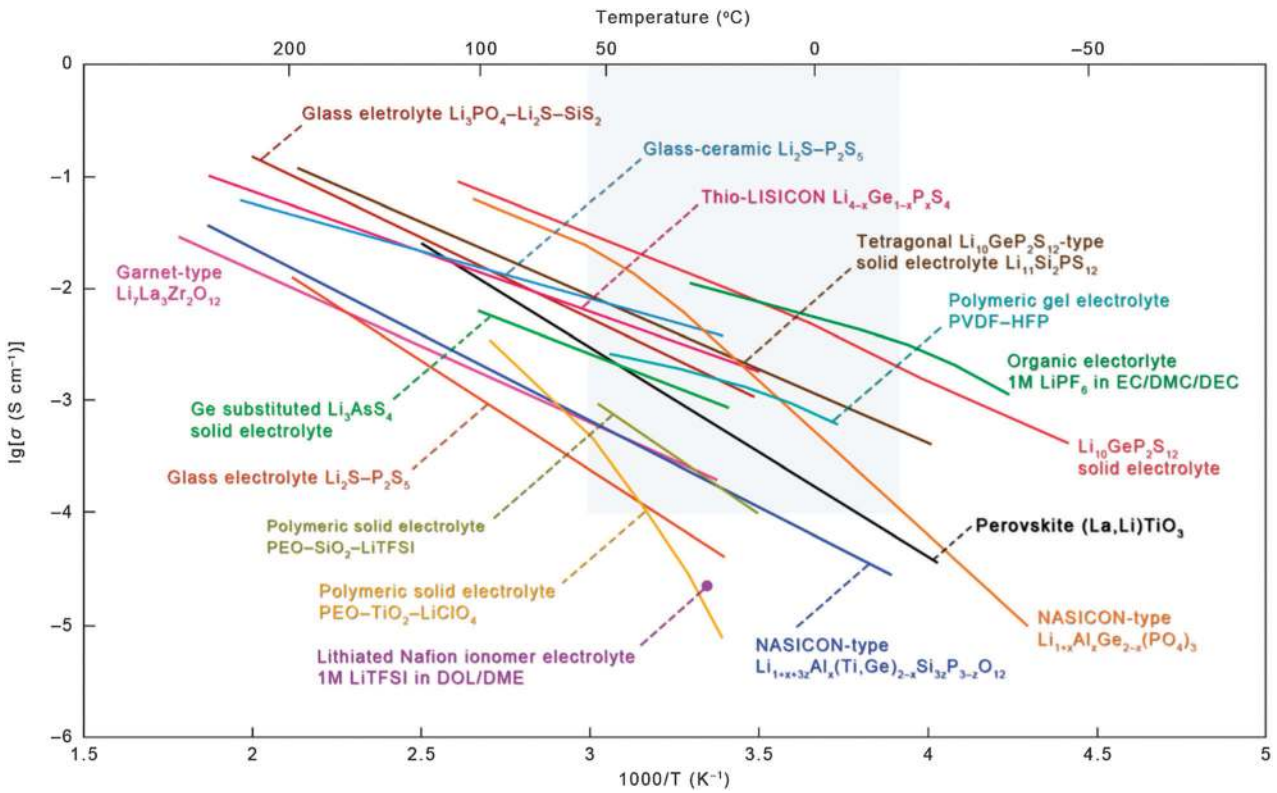

Fig. 24 Thermal evolution of ionic conductivity (σ) of the solid electrolytes and polymeric solid electrolytes. As a reference, the organic electrolyte adopted in Li-ion batteries is also included. The grey region indicates the ionic conductivity and temperature range suitable for Li-redox flow battery applications.

Table 5 Reported redox couples and their electrochemical parameters in Li-redox flow batteries

Cell chemistry	Cell type	Cell voltage (V)	Redox media of the catholyte	Bulk energy density[a] (W h kg^{-1})	Demonstrated energy density[b]	Ref.
$Fe(NO_3)_3$|Li	Flow	3.3	Aqueous, strong acidic	~1105	8–9 W h kg^{-1}	35
$K_3Fe(CN)_6$|Li	Static	3.4	Aqueous, weak alkaline	~276	8–9 W h kg^{-1}	34
	Flow	3.5			8–9 W h kg^{-1}	42
I_2|Li	Static	3.5	Aqueous, neutral	~726	330 W h kg^{-1}	36 and 62
	Flow				280 W h kg^{-1}	61
LiBr|Li	Static	4.0	Aqueous, weak acidic	~1320	30 W h kg^{-1}	37
$KMnO_4$|Zn	Static	2.8	Aqueous, strong acidic	~450	N/A	32
Cu|Li	Static	3.2	Aqueous, weak alkaline	~2440	30 W h kg^{-1}	38
Li_2S|Li	Static	2.5	Aqueous, strong alkaline	~650	14 W h kg^{-1}	40
Fc1N112-TFSI|Li	Flow	3.3	EC/PC/EMC	~160	50 W h L^{-1}	127
Ferrocene|Li	Static	3.6	DMF	~520	9–10 W h kg^{-1}	104
BQ|Li	Static	2.5–2.8	γ-Butyrolactone	~1240	5–6 W h kg^{-1}	177
2,5-Diethoxy-1,4-benzoquinone|Li	Static	2.6–2.8	γ-Butyrolactone	~510	18 W h kg^{-1}	177
2,5-Dipropoxy-1,4-benzoquinone|Li	Static	2.5–2.7	γ-Butyrolactone	~560	13 W h kg^{-1}	177
Polysulfide|Li	Static	2.3	DOL/DME	~260	97 W h kg^{-1}	103
15G3DAQ|Li	Static	2.1–2.4	PC	~210	25 W h L^{-1}	178
TiO_2 (suspension)|Li	Flow	1.0–1.7	PC	N/A	0.8 W h kg^{-1}	126
$LiFePO_4$ (suspension)|Li	Flow	3.2	EC/DMC	N/A	3.5 W h L^{-1}	124
DBBB|2,3,6-trimethylquinoxaline	Flow	1.3–1.7	PC	~80	12 W h L^{-1}	19
Polysulfide (suspension)|Li	Static	1.9–2.4	Tetraethylene glycol dimethyl ether	~2560	234 W h L^{-1}	168
	Flow				34 W h L^{-1}	
TEMPO|*N*-methylphthalimide	Static	1.0–1.4	Acetonitrile	~120	15 W h kg^{-1}	188
TEMPO|Li	Flow	2.7–3.2	EC/PC/EMC	~510	126 W h L^{-1}	189

[a] Based on the active material only. [b] Based on the total weight or volume of the catholyte and anode/anolyte.

electrochemical parameters in Li-redox flow batteries are summarized in Table 5.

Currently, metallic lithium has been employed as the anode in most cells because it has the highest specific capacity and the lowest anode potential of all. However, the lithium anode forms dendritic and mossy metal deposits, leading to serious safety concerns and low Coulombic efficiency during charge/discharge cycles.[21] Recent investigations to improve the stability of lithium anode involve interfacial engineering, surface passivation and integration of a buffer layer between lithium and electrolyte.[58,243,263–269]

The practical application of Li-redox flow batteries also depends on the development of redox-active materials, particularly the redox-active materials for the anolyte.[24] The choices of inorganic redox-active materials are rather limited. In contrast, the choices of organic materials should be rich enough to provide sufficient redox-active molecules in a broad potential window. Conjugated dicarboxylates have been widely studied in organic Li-ion batteries.[176,270,271] Conjugated polymeric Schiff base, thiophenes and multi-ring aromatics emerged recently have provided other clues for Li-redox flow battery anode application.[272–274] Suspensions of electroactive species with multiple redox moieties are also of great interest.[27,126,275] The structure diversity of organic electrode materials may further allow the tailoring of redox potential, solubility and electrochemical activity by introducing proper electron-donating/accepting functional groups. Other choices would rely on metallorganic compounds, of which the transition metal ions can reversibly transform their valence state with desired redox potential while maintaining structural stability. Metallocenes and electron-reservoir complexes might be good choices for both cathode and anode. For instance, the electron-reservoir complexes of $[(\eta^5\text{-}C_5H_5)Fe(\eta^6\text{-}C_6Me_6)]$ and $[(\eta^5\text{-}C_5Me_5)Fe(\eta^6\text{-}C_6Me_6)]$ show a redox potential of 1.5 and 1.2 V *vs.* Li^+/Li, respectively;[128] and the colbaltocene and decamethylcobaltocene also show a relatively low redox potential about 1.9 V and 1.3 V *vs.* Li^+/Li, respectively,[276,277] considerably lower than those used in Li-redox flow cells,[19,170,193,278] thus contributing to achieve optimized cell voltage. Potential candidates for redox-active anode material are summarized in Table 6.

Improvements in energy density and redox kinetics may be realized by increasing the solubility *via* molecular design and electrolyte choice. A facile redox reaction in catholyte or anolyte also depends on the current collector design. The general criteria for an ideal current collector are that it should provide good electric conductivity, exhibit good stability towards the interfacial redox reaction, and facilitate the diffusion of active species within the electrode.[62] Since most of the redox reactions adopted in Li-redox flow cells are facile, graphitic carbon materials meet such basic requirement.[15] Nevertheless, the physical properties of current collector, such as morphology, surface area and porosity do affect the final electrochemical performance of the cell. Particularly, for those redox reactions with poor redox kinetics, the assistance of catalysts or post-treatments of an optimized current collector will be necessary to facilitate the reaction process.[279–281]

Alike conventional redox flow batteries, Li-redox flow batteries should be more durable than conventional battery systems based on solid electrode configuration since the redox reactions proceed at solid (current collector)/liquid (electrolyte) interface, thus should not be accompanied by morphological/structural changes which is common in bulk electrodes due to the insertion or removal of electroactive species. Li-redox flow batteries should also be more scalable without sacrificing

Table 6 Potential redox active materials for the anolyte of Li-redox cells

Compound	Examples	Redox potential (V *vs.* Li^+/Li)	Bulk capacity (A h kg^{-1})	Ref.
Conjugated dicarboxylate	Di-lithium *trans–trans*-muconate	~1.4	348.1	175
	Di-lithium terephthalate	~1	301.1	175 and 270
	2,5-Dihydroxyterephthalic acid	~0.8	241.6	271
	4,4′-Tolane-dicarboxylate	~0.7	202.9	176
Conjugated polymeric Schiff base	Poly-[*N*,*N*′-*p*-(benzylidene)-*p*-phenylenediamine]	~1	324.7	272
Thiophene	n-Type poly(3,4-dihexylthiophene)	~0.5	117.3	273
Multi-ring aromatic	Naphthalene	0–1	1687	274
Metallocene	Cobaltocene	~1.8	141.7	276
	Decamethylcobaltocene	~1.3	81.4	277
Electron-reservoir complex	$[(\eta^5\text{-}C_5H_5)Fe(\eta^6\text{-}C_6Me_6)]$	~1.5	94.7	128
	$[(\eta^5\text{-}C_5Me_5)Fe(\eta^6\text{-}C_6Me_6)]$	~1.2	81.5	128
Suspension	Anatase TiO_2	1.5–2	N/A	126
	$Li_4Ti_5O_{12}$	~1.5	175	27

energy density and power density than conventional solid state batteries because the former may be readily modulated by varying the external circulating sub-systems. Moreover, Li-redox flow batteries are more flexible in design than conventional redox flow batteries since the cell can be configured with aqueous/aprotic hybrid electrolytes, or aprotic/aprotic hybrid electrolytes, or single component aprotic electrolytes, which enables great flexibility in choosing redox couples and supported electrolytes. Additionally, Li-redox flow batteries are not restricted to the existing inorganic redox couples. The cooperation of aprotic electrolytes and the structural diversity of organic and organometallic electrode materials would provide a number of choices for the cathode and the anode. It is expected that this new battery technology would stimulate the development of new electrochemical storage systems, as well as interdisciplinary collaborations that bring physics, chemistry, materials science and engineering, and computational science to the electrochemical arena.

Abbreviations

DEC	Diethyl carbonate
DMA	*N*,*N*-Dimethylacetamide
DME	Dimethoxyethane
DMF	*N*,*N*-Dimethylformamide
DMSO	Dimethyl sulfoxide
DOL	1,3-Dioxolane
EC	Ethylene carbonate
EMC	Ethyl methyl carbonate
HOMO	Highest occupied molecular orbital
LiTFSI	Lithium bis(trifluoromethanesulfonyl)imide
LISICON	Li^+ superionic conductor
LUMO	Lowest unoccupied molecular orbital
NASICON	Na^+ superionic conductor
OER	Oxygen evolution reaction
ORR	Oxygen reduction reaction
PC	Propylene carbonate
PVDF	Poly(vinyldifluoride)
SCE	Saturated calomel electrode
SHE	Standard hydrogen electrode
TCNQ	7,7,8,8-Tetracyanoquinodimethane
THF	Tetrahydrofuran

Acknowledgements

G.Y. acknowledges the financial support of faculty start up grant from the University of Texas at Austin and the Welch Foundation grant (F-1861). J.B.G. acknowledges the support by the Welch Foundation (F-1066). H.R.B. acknowledge the financial support from RIKEN. Y.Z. acknowledges the support from National Basic Research Program of China (Grant No. 2012CB932400) and the Major Research Plan of the National Natural Science Foundation of China (Grant No. 91333208).

Notes and references

1 http://www.ease-storage.eu/Technical_Documents.html, accessed: 2015.
2 M. Winter and R. J. Brodd, *Chem. Rev.*, 2004, **104**, 4245–4269.
3 M. Armand and J.-M. Taraascon, *Nature*, 2008, **451**, 652–657.
4 M. Armand, F. Endres, D. R. MacFarlane, H. Ohno and B. Scrosati, *Nat. Mater.*, 2009, **8**, 621–629.
5 M. S. Whittingham, *MRS Bull.*, 2008, **33**, 411–419.
6 J. B. Goodenough, *J. Solid State Electrochem.*, 2012, **16**, 2019–2029.
7 C. Ponce de León, A. Frías-Ferrer, J. González-García, D. A. Szánto and F. C. Walsh, *J. Power Sources*, 2006, **160**, 716–732.
8 M. R. Palacín, *Chem. Soc. Rev.*, 2009, **38**, 2565–2575.
9 J. Cabana, L. Monconduit, D. Larcher and M. R. Palacín, *Adv. Mater.*, 2010, **22**, E170–E192.
10 J. B. Goodenough and Y. Kim, *Chem. Mater.*, 2010, **22**, 587–603.
11 P. G. Bruce, S. A. Freunberger, L. J. Hardwick and J.-M. Taraascon, *Nat. Mater.*, 2012, **11**, 19–29.
12 N.-S. Choi, Z. Chen, S. A. Freunberger, X. Ji, Y.-K. Sun, K. Amine, G. Yushin, L. F. Nazar, J. Cho and P. G. Bruce, *Angew. Chem., Int. Ed.*, 2012, **51**, 9994–10024.
13 P. Leung, X. Li, C. P. De Leon, L. Berlouis, C. T. J. Low and F. C. Walsh, *RSC Adv.*, 2012, **2**, 10125–10156.
14 Z. Yang, J. Zhang, M. C. W. Kintner-Meyer, X. KLu, D. Choi, J. P. Lemmon and J. Liu, *Chem. Rev.*, 2011, **111**, 3577–3613.
15 A. Z. Webber, M. M. Mench, J. P. Meyers, P. N. Ross, J. T. Gostick and Q. Liu, *J. Appl. Electrochem.*, 2011, **41**, 1137–1164.

16 M. Skyllas-Kazacos, M. H. Chakrabarti, S. A. Hajimolana, F. S. Mjalli and M. Saleem, *J. Electrochem. Soc.*, 2011, **158**, R55–R79.
17 B. Dunn, H. Kamath and J.-M. Taraascon, *Science*, 2011, **334**, 928–935.
18 Y. Wang, P. He and H. Zhou, *Adv. Energy Mater.*, 2012, **2**, 770–779.
19 F. R. Brushett, J. T. Vaughey and A. N. Jansen, *Adv. Energy Mater.*, 2012, **2**, 1390–1396.
20 B. L. Ellis, K. T. Lee and L. F. Nazar, *Chem. Mater.*, 2010, **22**, 691–714.
21 M. S. Whittingham, *Chem. Rev.*, 2004, **104**, 4217–4302.
22 S. Flandrois and B. Simon, *Carbon*, 1999, **37**, 165–180.
23 P. Arora and Z. Zhang, *Chem. Rev.*, 2004, **104**, 4419–4462.
24 J. B. Goodenough, *Energy Environ. Sci.*, 2014, **7**, 14–18.
25 K. Xu, *Chem. Rev.*, 2004, **104**, 4303–4417.
26 X. Zhang, R. Kostecki, T. J. Richardson, J. K. Pugh and J. P. N. Ross, *J. Electrochem. Soc.*, 2001, **148**, A1341–A1345.
27 M. Duduta, B. Ho, V. C. Wood, P. Limthongkul, V. E. Brunini, W. C. Carter and Y.-M. Chiang, *Adv. Energy Mater.*, 2011, **1**, 511–516.
28 A. A. Shah, H. Al-Fetlawi and F. C. Walsh, *Electrochim. Acta*, 2010, **55**, 1125–1139.
29 M. Urquidi-Macdonald, J. Flores, D. D. Macdonald, O. Pensado-Rodrguez and D. Van Voorhis, *Electrochim. Acta*, 1998, **43**, 3069–3077.
30 E. L. Littauer and K. C. Tsai, *J. Electrochem. Soc.*, 1976, **123**, 771–776.
31 S. J. Visco, B. D. Katz, Y. S. Nimon and L. D. Dejonghe, *US Pat.*, 72822952007.
32 L. Chen, Z. Guo, Y. Xia and Y. Wang, *Chem. Commun.*, 2013, **49**, 2204–2206.
33 P. He, Y. Wang and H. Zhou, *Chem. Commun.*, 2011, **47**, 10701–10703.
34 Y. Lu, J. B. Goodenough and Y. Kim, *J. Am. Chem. Soc.*, 2011, **133**, 5756–5759.
35 Y. Wang, Y. Wang and H. Zhou, *ChemSusChem*, 2011, **4**, 1087–1090.
36 Y. Zhao, L. Wang and H. R. Byon, *Nat. Commun.*, 2013, **4**, 1896.
37 Y. Zhao, Y. Ding, J. Song, J. B. Goodenough and G. Yu, *Energy Environ. Sci.*, 2014, **7**, 1990–1995.
38 Y. Wang and H. Zhou, *Electrochem. Commun.*, 2009, **11**, 1834–1837.
39 E. Yoo and H. Zhou, *ACS Nano*, 2011, **5**, 3020–3026.
40 N. Li, Z. Weng, Y. Wang, F. Li, H.-M. Cheng and H. Zhou, *Energy Environ. Sci.*, 2014, **7**, 3307–3312.
41 D. R. Lide, *CRC Handbook of Chemistry and Physics*, CRC Press, LLC, Boca Raton, FL, 3rd edn, 2000.
42 Y. Lu and J. B. Goodenough, *J. Mater. Chem.*, 2011, **11**, 10113–10117.
43 T. Zhang, N. Imanishi, S. Hasegava, A. Hirano, J. Xie, Y. Takeda, O. Yamamoto and N. Sammes, *J. Electrochem. Soc.*, 2008, **155**, A965–A969.
44 L. Li, S. Kim, W. Wang, M. Vijayakumar, Z. Nie, B. Chen, J. Zhang, G. Xia, J. Z. Hu, G. L. Graff, J. Liu and Z. Yang, *Adv. Energy Mater.*, 2011, **1**, 394–400.
45 F. Ding, W. Xu, Y. Shao, X. Chen, Z. Wang, F. Gao, X. Liu and J.-G. Zhang, *J. Power Sources*, 2012, **214**, 292–297.
46 S. Hasegawa, N. Imanishi, T. Zhang, J. Xie, A. Hirano, Y. Takeda and O. Yamamoto, *J. Power Sources*, 2009, **189**, 371–377.
47 Y.-W. D. Chen, K. S. V. Santhanam and A. J. Bard, *J. Electrochem. Soc.*, 1982, **128**, 1460–1467.
48 T. Iwasita, W. Schmickler, J. Herrmann and U. Vogel, *J. Electrochem. Soc.*, 1983, **130**, 2026–2032.
49 Y. H. Wen, H. M. Zhang, P. Qian, H. T. Zhou, P. Zhao, B. L. Yi and Y. S. Yang, *Electrochim. Acta*, 2006, **51**, 3769–3775.
50 Y. H. Wen, H. M. Zhang, P. Qian, H. T. Zhou, P. Zhao, B. L. Yi and T. S. Yang, *J. Electrochem. Soc.*, 2006, **153**, A929–A934.
51 R. W. Ramette and R. W. J. Sandford, *J. Am. Chem. Soc.*, 1965, **87**, 5001–5005.
52 P. H. Svensson and L. Kloo, *Chem. Rev.*, 2003, **103**, 1649–1684.
53 M. J. Mader and R. E. White, *J. Electrochem. Soc.*, 1986, **133**, 1297–1307.
54 H. Kreutzer, V. Yarlagadda and T. V. Nguyen, *J. Electrochem. Soc.*, 2012, **159**, F331–F337.
55 Q. Lai, H. Zhang, X. Li, L. Zhang and Y. Cheng, *J. Power Sources*, 2013, **235**, 1–4.
56 C. Teng, X. C. Yang, C. Z. Yuan, C. Y. Li, R. K. Chen, H. N. Tian, S. F. Li, A. Hagfeldt and L. C. Sun, *Org. Lett.*, 2009, **11**, 5542–5545.
57 Z. Chang, X. Wang, Y. Yang, J. Gao, M. Li, L. Liu and Y. Wu, *J. Mater. Chem. A*, 2014, **2**, 19444–19450.
58 Y. Zhao, N. B. Mercier and H. R. Byon, *ChemPlusChem*, 2015, **80**, 344–348.
59 E. Kjeang, R. Michel, D. A. Harrington, N. Djilali and D. Sinton, *J. Am. Chem. Soc.*, 2008, **130**, 4000–4006.
60 E. Kjeang, J. McKechnie, D. Sinton and N. Djilali, *J. Power Sources*, 2007, **168**, 379–390.
61 Y. Zhao and H. R. Byon, *Adv. Energy Mater.*, 2013, **3**, 1630–1635.
62 Y. Zhao, M. Hong, N. B. Mercier, G. Yu, H. C. Choi and H. R. Byon, *Nano Lett.*, 2014, **14**, 1085–1092.
63 M. Skyllas-Kazacos, G. Kazacos, G. Poon and H. Verseema, *Int. J. Energy Res.*, 2010, **34**, 182–189.
64 X. Wang, Y. Hou, Y. Zhu, Y. Wu and R. Holze, *Sci. Rep.*, 2013, **3**, 1401.
65 C. P. De Leon, G. W. Reade, I. Whyte, S. E. Male and F. C. Walsh, *Electrochim. Acta*, 2007, **52**, 5815–5823.
66 Y. Shao, X. Wang, M. Engelhard, C. Wang, S. Dai, J. Liu, Z. Yang and Y. Lin, *J. Power Sources*, 2010, **195**, 4375–4379.
67 K. M. Abraham and Z. Jiang, *J. Electrochem. Soc.*, 1996, **143**, 1–5.
68 S. J. Visco, B. D. Katz, Y. S. Nimon and L. C. De Jonghe, *US Pat.*, 20070117007, 2007.
69 A. Manthiram and L. Li, *Adv. Energy Mater.*, 2015, **5**, 201401302.
70 Y. Shimonishi, T. Zhang, N. Imanishi, D. Im, D. J. Lee, A. Hirano, Y. Takeda, O. Yamamoto and N. Sammes, *J. Power Sources*, 2011, **196**, 5128–5132.
71 H. Ohkuma, I. Uechi, M. Matsui, Y. Takeda, O. Yamamoto and N. Imanishi, *J. Power Sources*, 2014, **245**, 947–952.
72 L. Li, X. Zhao and A. Manthiram, *Electrochem. Commun.*, 2012, **14**, 78–81.

73 Y. Shimonishi, T. Zhang, P. Johnson, N. Imanishi, A. Hirano, Y. Takeda, O. Yamamoto and N. Sammes, *J. Power Sources*, 2010, **195**, 6187–6191.
74 L. Li, Y. Fu and A. manthiram, *Electrochem. Commun.*, 2014, **47**, 67–70.
75 H. R. Byon, J. Suntivich and Y. Shao-Horn, *Chem. Mater.*, 2011, **23**, 3421–3428.
76 C. C. L. McCrory, S. Jung, J. C. Peters and T. F. Jaramillo, *J. Am. Chem. Soc.*, 2013, **135**, 16977–16987.
77 Z.-L. Wang, D. Xu, J.-J. Xu and X.-B. Zhang, *Chem. Soc. Rev.*, 2014, **43**, 7746–7786.
78 R. Cao, J.-S. Lee, M. Liu and J. Cho, *Adv. Energy Mater.*, 2012, **2**, 816–829.
79 H. Zhou, Y. Wang, H. Li and P. He, *ChemSusChem*, 2010, **3**, 1009–1019.
80 T. Sakai, T. Iwaki, Z. Ye and D. Noréus, *J. Electrochem. Soc.*, 1995, **142**, 4040–4045.
81 Y.-C. Lu, Z. Xu, H. A. Gasteiger, S. Chen, K. Hamad-Schifferli and Y. Shao-Horn, *J. Am. Chem. Soc.*, 2010, **132**, 12170–12171.
82 J. Suntivich, H. A. Gasteiger, N. Yabuuchi, H. Nakanishi, J. B. Goodenough and Y. Shao-Horn, *Nat. Chem.*, 2011, **3**, 546–550.
83 J. Suntivich, K. J. May, H. A. Gasteiger, J. B. Goodenough and Y. Shao-Horn, *Science*, 2011, **334**, 1383–1385.
84 W. Yang, J. Salim, S. Li, C. Sun, L. Chen, J. B. Goodenough and Y. Kim, *J. Mater. Chem.*, 2012, **22**, 18902–18907.
85 Y. Liang, Y. Li, H. Wang, J. Zhou, J. Wang, T. Regier and H. Dai, *Nat. Mater.*, 2011, **10**, 780–786.
86 L. Li, S.-H. Chai, S. Dai and A. Manthiram, *Energy Environ. Sci.*, 2014, **7**, 2630–2636.
87 B. O'Regan and M. Grätzel, *Nature*, 1991, **353**, 737–740.
88 J. H. Alstrum-Acevedo, M. K. Brennaman and T. J. Meyer, *Inorg. Chem.*, 2005, **44**, 6802–6827.
89 W. Song, Z. Chen, M. K. Brennaman, J. J. Concepcion, A. O. Patrocinio, N. Y. Murakami Iha and T. J. Meyer, *Pure Appl. Chem.*, 2011, **83**, 749–768.
90 T. J. Meyer, *Nat. Chem.*, 2011, **3**, 757–758.
91 A. Hagfeldt, G. Boschloo, L. Sun, L. Kloo and H. Pettersson, *Chem. Rev.*, 2010, **110**, 6595–6663.
92 G. Boschlii and A. Hagfeldt, *Acc. Chem. Res.*, 2009, **42**, 1819–1826.
93 N. F. Yan, G. R. Li and X. P. Gao, *J. Mater. Chem. A*, 2013, **1**, 7012–7015.
94 N. F. Yan, G. R. Li and X. P. Gao, *J. Electrochem. Soc.*, 2014, **161**, A736–A741.
95 A. B. F. Martinson, T. W. Hamann, M. J. Pellin and J. T. Hupp, *Chem. – Eur. J.*, 2008, **14**, 4458–4467.
96 M. H. Chakrabarti, R. A. W. Dryfe and E. P. L. Roberts, *Electrochim. Acta*, 2007, **52**, 2189–2195.
97 S.-H. Shin, S.-H. Yun and S.-H. Moon, *RSC Adv.*, 2013, **3**, 9095–9116.
98 Y. Matsuda, K. Tanaka, M. Okada, Y. Takasu and M. Morita, *J. Appl. Electrochem.*, 1988, **18**, 909–914.
99 J.-H. Kim, K. J. Kim, M.-S. Park, N. J. Lee, U. Hwang, H. Kim and Y.-J. Kim, *Electrochem. Commun.*, 2011, **13**, 997–1000.
100 Q. Liu, A. A. Shinkle, Y. Li, C. W. Monroe, L. T. Thompson and A. E. S. Sleightolme, *Electrochem. Commun.*, 2010, **12**, 1634–1637.
101 Q. Liu, A. E. S. Sleightolme, A. A. Shinkle, Y. Li and L. T. Thompson, *Electrochem. Commun.*, 2009, **11**, 2312–2315.
102 A. E. S. Sleightolme, A. A. Shinkle, Q. Liu, Y. Li, C. W. Monroe and L. T. Thompson, *J. Power Sources*, 2011, **196**, 5742–5745.
103 Y. Yang, G. Zheng and Y. Cui, *Energy Environ. Sci.*, 2013, **6**, 1552–1558.
104 Y. Zhao, Y. Ding, J. Song, G. Li, G. Dong, J. B. Goodenough and G. Yu, *Angew. Chem., Int. Ed.*, 2014, **53**, 11036–11040.
105 D. Astruc, *Organometallic chemistry and catalysis*, Springer, Berlin Heidelberg, 2007.
106 M. A. Vorotyntsev, M. Casalta, E. Pousson, L. Roullier, G. Boni and C. Moise, *Electrochim. Acta*, 2001, **46**, 4017–4033.
107 W. E. Geiger Jr., *J. Am. Chem. Soc.*, 1974, **96**, 2632–2634.
108 D. Chong, J. Slote and W. E. Geiger, *J. Electroanal. Chem.*, 2009, **630**, 28–34.
109 I. Noviandri, K. N. Brown, D. S. Fleming, P. T. Gulyas, P. A. Lay, A. F. Masters and L. Phillips, *J. Phys. Chem. B*, 1999, **103**, 6713–6722.
110 J. C. Smart and J. L. Robbins, *J. Am. Chem. Soc.*, 1978, **100**, 3936–3938.
111 N. El Murr, J. E. Sheats, W. E. Geiger Jr. and J. D. L. Holloway, *Inorg. Chem.*, 1979, **18**, 1443–1446.
112 J. D. L. Holloway, W. L. Bowden and W. E. Geiger Jr., *J. Am. Chem. Soc.*, 1977, **99**, 7089–7090.
113 M. N. Golovin, D. P. Wilkinson, J. T. Dudley, D. Holonko and S. Woo, *J. Electrochem. Soc.*, 1992, **139**, 5–10.
114 K.-S. Park, S. B. Schougaard and J. B. Goodenough, *Adv. Mater.*, 2007, **19**, 848–851.
115 D. Astruc, C. Ornelas and J. Ruiz, *Chem. – Eur. J.*, 2009, **15**, 8936–8944.
116 Y. Ding, Y. Zhao and G. Yu, *Nano Lett.*, 2015, **15**, 4108–4113.
117 A. S. Baranski and K. Winkler, *J. Electroanal. Chem.*, 1991, **313**, 367–375.
118 Y. Wang, E. I. Rogers and R. G. Compton, *J. Electroanal. Chem.*, 2010, **648**, 15–19.
119 R. M. Nielson, G. E. McManis, L. K. Safford and M. J. Weaver, *J. Phys. Chem.*, 1989, **93**, 2152–2157.
120 E. S. Yang, M.-S. Chan and A. C. Wahl, *J. Phys. Chem.*, 1975, **79**, 2049–2052.
121 E. S. Yang, M.-S. Chan and A. C. Wahl, *J. Phys. Chem.*, 1980, **84**, 3094–3099.
122 V. M. Hultgren, A. W. A. Mariotti, A. M. Bond and A. G. Wedd, *Anal. Chem.*, 2002, **74**, 3151–3156.
123 A. G. Marrani, F. Cattaruzza, F. Decker, P. Galloni and R. Zanoni, *Electrochim. Acta*, 2010, **55**, 5733–5740.
124 Q. Huang, L. Li, M. Grätzel and Q. Wang, *Phys. Chem. Chem. Phys.*, 2013, **15**, 1793–1797.
125 Q. Wang, S. M. Zakeeruddin, D. Wang, I. Exnar and M. Grätzel, *Angew. Chem., Int. Ed.*, 2006, **45**, 8197–8200.
126 F. Pan, J. Yang, Q. Huang, X. Wang, H. Huang and Q. Wang, *Adv. Energy Mater.*, 2014, **5**, 1400567.

127 X. Wei, L. Cosimbescu, W. Xu, J. Z. Hu, M. Vijayakumar, J. Feng, M. Y. Hu, X. Deng, J. Xiao, J. Liu, V. Sprenkle and W. Wang, *Adv. Energy Mater.*, 2015, **5**, 1400678.
128 D. Astruc, *New J. Chem.*, 2009, **33**, 1191–1206.
129 N. Jayaprakash, J. Shen, S. S. Moganty, A. Corona and L. A. Archer, *Angew. Chem., Int. Ed.*, 2011, **50**, 5904–5908.
130 L. Wang, Y. Zhao, M. L. Thomas and H. R. Byon, *Adv. Funct. Mater.*, 2014, **24**, 2248–2252.
131 J. Guo, Z. Yang, Y. Yu, H. D. Abruña and L. A. Archer, *J. Am. Chem. Soc.*, 2013, **135**, 763–767.
132 Z. W. Seh, W. Li, J. J. Cha, G. Zheng, Y. Yang, M. T. McDowell, P.-C. Hsu and Y. Cui, *Nat. Commun.*, 2012, **4**, 1331.
133 R. D. Rauh, F. S. Shuker, J. M. Marston and S. B. Brummer, *J. Inorg. Nucl. Chem.*, 1977, **39**, 1761–1766.
134 M. Cuisinier, P.-E. Cabelguen, S. Evers, G. He, M. Kolbeck, A. Garsuch, T. Bolin, M. Balasubramanian and L. F. Nazar, *J. Phys. Chem. Lett.*, 2013, **4**, 3227–3232.
135 S. Waluś, C. Barchasz, J.-F. Colin, J.-F. Martin, E. Elkaïm, J.-C. Leprêtre and F. Alloin, *Chem. Commun.*, 2013, **49**, 7899–7901.
136 K. A. See, M. Leskes, J. M. Griffin, S. Britto, P. D. Mathews, A. Emly, A. Van der Ven, D. S. Wright, A. J. Morris, C. P. Grey and R. Seshadri, *J. Am. Chem. Soc.*, 2014, **136**, 16368–16377.
137 J. Nelson, S. Misra, Y. Yang, A. Jackson, Y. Liu, H. Wang, H. Dai, J. C. Andrews, Y. Cui and M. F. Toney, *J. Am. Chem. Soc.*, 2012, **134**, 6337–6343.
138 Z. H. Li, L. Yuan, Z. Yi, Y. Y. Sun, Y. Liu, Y.-B. Jiang, Y. Shen, Y. Xin, Z. Zhang and Y. Huang, *Adv. Energy Mater.*, 2013, **4**, 1301473.
139 C. Barchasz, F. Molton, C. Duboc, J.-C. Leprêtre, S. Patoux and F. Alloin, *Anal. Chem.*, 2012, **84**, 3973–3980.
140 Y.-C. Lu, Q. He and H. A. Gasteiger, *J. Phys. Chem. C*, 2014, **118**, 5733–5741.
141 R. D. Rauh, K. M. Abraham, G. F. Pearson, J. K. Surprenant and S. B. Brummer, *J. Electrochem. Soc.*, 1979, **126**, 523–527.
142 S. S. Zhang and J. A. Read, *J. Power Sources*, 2012, **200**, 77–82.
143 T. Yim, M.-S. Park, J.-S. Yu, K. J. Kim, K. Y. Im, J.-H. Kim, G. Jeong, Y. N. Jo, S.-G. Woo, K. S. Kang, I. Lee and Y.-J. Kim, *Electrochim. Acta*, 2013, **107**, 454–460.
144 J. Gao, M. A. Lowe, Y. Kiya and H. D. Abruña, *J. Phys. Chem. C*, 2011, **115**, 25132–25137.
145 F. Carey and R. Sundberg, *Advanced Organic Chemistry*, Springer, New York, 2007.
146 R. D. Rauh, F. S. Shuker, J. M. Martston and S. B. Brummer, *J. Inorg. Nucl. Chem.*, 1977, **39**, 1761–1766.
147 S.-I. Tobishima, H. Yamamoto and M. Matsuda, *Electrochim. Acta*, 1997, **42**, 1019–1029.
148 X. Ji, K. T. Lee and L. F. Nazar, *Nat. Mater.*, 2009, **8**, 500–506.
149 Y. Yang, G. Zheng and Y. Cui, *Chem. Soc. Rev.*, 2013, **42**, 3018–3032.
150 A. Manthiram, Y. Fu, S.-H. Chung, C. Zu and Y.-S. Su, *Chem. Rev.*, 2014, **114**, 11751–11787.
151 X. Ji and L. F. Nazar, *J. Mater. Chem.*, 2010, **20**, 9821–9826.
152 T. Kobayashi, Y. Imade, D. Shishihara, K. Homma, M. Nagao, R. Watanabe, T. Yokoi, A. Yamada, R. Kanno and T. Tatsumi, *J. Power Sources*, 2008, **182**, 621–625.
153 M. Nagao, Y. Imade, H. Narisawa, T. Kobayashi, R. Watanabe, T. Yokoi, T. Tatsumi and R. Kanno, *J. Power Sources*, 2013, **222**, 237–242.
154 A. Hayashi, T. Ohtomo, F. Mizuno, K. Tadanaga and M. Tatsumisago, *Electrochem. Commun.*, 2003, **5**, 701–705.
155 T. Hakari, M. Nagao, A. Hayashi and M. Tatsumisago, *Solid State Ionics*, 2014, **262**, 147–150.
156 Y.-Z. Fu, Y.-S. Su and A. Manthiram, *Angew. Chem., Int. Ed.*, 2013, **52**, 6930–6935.
157 H. Yao, G. Zheng, P.-C. Hsu, D. Kong, J. J. Cha, W. Li, Z. W. Seh, M. T. McDowell, K. Yan, Z. Liang, V. K. Narasimhan and Y. Cui, *Nat. Commun.*, 2014, **5**, 3943.
158 R. Demir-Cakan, M. Morcrette, Gangulibabu, A. Guéguen, R. Dedryvère and J.-M. Taraascon, *Energy Environ. Sci.*, 2013, **6**, 176–182.
159 S.-H. Chung and A. Manthiram, *Adv. Mater.*, 2014, **26**, 1360–1365.
160 C. Zu and A. Manthiram, *Adv. Energy Mater.*, 2014, **4**, 1400897.
161 X. Ji, S. Evers, R. Black and L. F. Nazar, *Nat. Commun.*, 2011, **2**, 325.
162 C. Zu, Y. Fu and A. Manthiram, *J. Mater. Chem. A*, 2013, **1**, 10362–10367.
163 X. Han, Y. Xu, X. Chen, Y.-C. Chen, N. Weadock, J. Wan, H. Zhu, Y. Liu, H. Li, G. Rubloff, C. Wang and L. Hu, *Nano Energy*, 2013, **2**, 1197–1206.
164 Y.-S. Su and A. Manthiram, *Chem. Commun.*, 2012, **48**, 8817–8819.
165 A. Gorkovenko, T. A. Skotheim and Z.-S. Xu, *Cathodes Comprising Electroactive Sulfur Materials and Secondary Batteries Using Same*, US Pat., 6,878,488, 812, 2005.
166 Y. Fu, Y.-S. Su and A. Manthiram, *Adv. Energy Mater.*, 2014, **4**, 1300655.
167 G. Zhou, S. Pei, D.-W. Wang, S. Wang, K. Huang, L.-C. Yin, F. Li and H.-M. Cheng, *Adv. Mater.*, 2014, **26**, 625–631.
168 F. Y. Fan, W. H. Woodford, Z. Li, N. Baram, K. C. Smith, A. Helal, G. H. McKinley, W. C. Carter and Y.-M. Chiang, *Nano Lett.*, 2014, **14**, 2210–2218.
169 N. Li, Y. Wang, D. Tang and H. Zhou, *Angew. Chem., Int. Ed.*, 2015, **54**, 9271–9274.
170 Z. Song and H. Zhou, *Energy Environ. Sci.*, 2013, **6**, 2280–2301.
171 Y. Liang, Z. Tao and J. Chen, *Adv. Energy Mater.*, 2012, **2**, 742–769.
172 T. Suga, H. Ohshiro, S. Sugita, K. Oyaizu and H. Nishide, *Adv. Mater.*, 2009, **21**, 1627–1630.
173 H. G. Aurich, *Nitrones, Nitronates and Nitroxide*, John Wiley & Sons, New York, 1989.
174 L. B. Volodarsky, V. A. Reznikov and V. I. Ovcharenko, *Synthetic Chemistry of Stable Nitroxides*, CRC Press, Boca Raton, FL, 1994.
175 M. Armand, H. Vezin, S. Laruelle, P. Ribière, P. Poizot and J.-M. Tarascon, *Nat. Mater.*, 2009, **8**, 120–125.

176 W. Walker, S. Grugeon, H. Vezin, S. Laruelle, M. Armand, F. Wudl and J.-M. Tarascon, *J. Mater. Chem.*, 2011, **21**, 1615–1620.
177 H. Senoh, M. Yao, H. Sakaebe, K. Yasuda and Z. Siroma, *Electrochim. Acta*, 2011, **56**, 10145–10150.
178 W. Wang, W. Xu, L. Cosimbescu, D. Choi, L. Li and Z. Yang, *Chem. Commun.*, 2012, **48**, 6669–6671.
179 H. Nishide, K. Koshika and K. Oyaizu, *Pure Appl. Chem.*, 2009, **81**, 1961–1970.
180 T. Janoschka, M. D. Hager and U. S. Schubert, *Adv. Mater.*, 2012, **24**, 6397–6490.
181 T. Suga, Y. J. Pu, K. Oyaizu and H. Nishide, *Bull. Chem. Soc. Jpn.*, 2004, **77**, 2203–2204.
182 J. L. Hodgson, M. Namazian, S. E. Bottle and M. L. Coote, *J. Phys. Chem. A*, 2007, **111**, 13595–13605.
183 C. Buhrmester, L. M. Moshurchak, R. L. Wang and J. R. Dahn, *J. Electrochem. Soc.*, 2006, **153**, A1800–A1804.
184 P. Nesvadba, L. Bugnon, P. Maire and P. Novák, *Chem. Mater.*, 2010, **22**, 783–788.
185 T. Suga, Y. J. Pu, S. Kasatori and H. Nishide, *Macromolecules*, 2007, **40**, 3167–3173.
186 T. Suga, S. Sugita, H. Ohshiro, K. Yoyaizu and H. Nishide, *Adv. Mater.*, 2011, **23**, 751–754.
187 J. Qu, T. Fujii, T. Katsumata, Y. Suzuki, M. Shiotsuki, F. Sanda, M. Satoh, J. Wada and T. Masuda, *J. Polym. Sci., Part A: Polym. Chem.*, 2007, **45**, 5431–5445.
188 Z. Li, S. Li, S. Liu, K. Huang, D. Fang, F. Wang and S. Peng, *Electrochem. Solid-State Lett.*, 2011, **14**, A171–A173.
189 X. Wei, W. Xu, M. Vijayakumar, L. Cosimbescu, T. Liu, V. Sprenkle and W. Wang, *Adv. Mater.*, 2014, **26**, 7649–7653.
190 T. Nokami, T. Matsuo, Y. Inatomi, N. Hojo, T. Tsukagoshi, H. Yashizawa, A. Shimizu, H. Kuramoto, K. Komae, H. Tsuyama and J.-i. Yoshida, *J. Am. Chem. Soc.*, 2012, **134**, 19694–19700.
191 N. Oyama, T. Tatsuma, T. Sato and T. Sotomura, *Nature*, 1995, **373**, 598–600.
192 Z. Song, T. Xu, M. Gordin, Y.-B. Jiang, I.-T. Bae, Q. Xiao, H. Zhan, J. Liu and D. Wang, *Nano Lett.*, 2012, **12**, 2205–2211.
193 B. Huskinson, M. P. Marshak, C. Suh, S. Er, M. R. Gerhardt, C. J. Galvin, X. Chen, A. Aspuru-Guzik, R. G. Gordon and M. J. Aziz, *Nature*, 2014, **505**, 195–198.
194 M. Adachi, K. Tanaka and K. Sekai, *J. Electroanal. Chem.*, 1999, **146**, 1256–1261.
195 J. R. Dahn, J. Jiang, L. M. Moshurchak, M. D. Fleischauer, C. Buhrmester and L. J. Krause, *J. Electrochem. Soc.*, 2005, **152**, A1283–A1289.
196 G. Dantsin, K. Jambunathan, S. V. Ivanov, W. J. Casteel, K. Amine, J. Liu, A. N. Jansen and Z. Chen, *208th ECS Meeting Abstracts, Los Angeles, CA*, 2005 (Abstract No. 2223).
197 S. S. Zhang, *J. Power Sources*, 2006, **162**, 1379–1394.
198 R. J. Gale and R. Job, *Inorg. Chem.*, 1981, **20**, 40–42.
199 J. B. Goodenough, Y. H.-P. Hong and J. A. Kafalas, *Mater. Res. Bull.*, 1976, **11**, 203–220.
200 H. Aono, *Acc. Chem. Res.*, 1994, **27**, 265–270.
201 H. Aono and E. Sugimoto, *J. Electrochem. Soc.*, 1989, **136**, 590–591.
202 G.-y. Adachi, N. Imanishi and H. Aono, *Adv. Mater.*, 1996, **8**, 127–135.
203 H. Aono, E. Sugimoto, Y. Sadaoka, N. Imanishi and G.-y. Adachi, *Chem. Lett.*, 1990, 331–334.
204 Y. Li, M. Liu, K. Liu and C.-A. Wang, *J. Power Sources*, 2013, **240**, 50–53.
205 H. Xie, J. B. Goodenough and Y. Li, *J. Power Sources*, 2011, **196**, 7760–7762.
206 Y. Li, J.-T. Han, C.-A. Wang, S. C. Vogel, H. Xie, M. Xu and J. B. Goodenough, *J. Power Sources*, 2012, **209**, 278–281.
207 Y. Li, J.-T. Han, C.-A. Wang, H. Xie and J. B. Goodenough, *J. Mater. Chem.*, 2012, **22**, 15357–15361.
208 H. Xie, J. A. Alonso, Y. Li, M. T. Fernández-Díaz and J. B. Goodenough, *Chem. Mater.*, 2011, **23**, 3587–3589.
209 S. Ohta, T. Kobayashi and T. Asaoka, *J. Power Sources*, 2011, **196**, 3342–3345.
210 Y. Li, C.-A. Wang, H. Xie, J. Cheng and J. B. Goodenough, *Electrochem. Commun.*, 2011, **13**, 1289–1292.
211 Y. Jin and P. J. McGinn, *J. Power Sources*, 2011, **196**, 8683–8687.
212 C. Bernuy-Lopez, W. Manalastas, J. M. Lopez del Amo, A. Aguadero, F. Aguesse and J. A. Kilner, *Chem. Mater.*, 2014, **26**, 3610–3617.
213 C. Galven, J. Dittmer, E. Suard, F. Le Berre and M.-P. Crosnier-Lopez, *Chem. Mater.*, 2012, **24**, 3335–3345.
214 L. Truong, M. Howard, O. Clemens, K. S. Knight, P. R. Slater and V. Thangadurai, *J. Mater. Chem. A*, 2013, **1**, 13469–13475.
215 S. Stramare, V. Thangadurai and W. Weppner, *Chem. Mater.*, 2003, **15**, 3974–3990.
216 C. H. Chen, S. Xie, E. Sperling, A. S. Yang, G. Henriksen and K. Amine, *Solid State Ionics*, 2004, **167**, 263–272.
217 R. Inada, K. Kimura, K. Kusakabe, T. Tojo and Y. Sakurai, *Solid State Ionics*, 2014, **261**, 95–99.
218 Y. Zhao and L. L. Daemen, *J. Am. Chem. Soc.*, 2012, **134**, 15042–15047.
219 D. J. Schroeder, A. A. Hubaud and J. T. Vaughey, *Mater. Res. Bull.*, 2014, **49**, 614–617.
220 A. Emly, E. Kioupakis and A. Van der Ven, *Chem. Mater.*, 2013, **25**, 4663–4670.
221 R. V. Morford, D. T. Welna, C. E. Kellam III, M. A. Hofmann and H. R. Allcock, *Solid State Ionics*, 2006, **177**, 721–726.
222 T.-H. Cho, M. Tanaka, H. Onishi, Y. Kondo, T. Nakamura, H. Hiroaki, S. Tanase and T. Sakai, *J. Power Sources*, 2008, **181**, 155–160.
223 H. P. Zhang, P. Zhang, Z. H. Li, M. Sun, Y. P. Wu and H. Q. Wu, *Electrochem. Commun.*, 2007, **9**, 1700–1703.
224 M. G. Buonomenna, P. Macchi, M. Davoli and E. Drioli, *Eur. Polym. J.*, 2007, **43**, 1557–1572.
225 C. M. Costa, J. L. Gomez Ribelles, S. Lanceros-Méndez, G. B. Appetecchi and B. Scrosati, *J. Power Sources*, 2014, **245**, 779–786.
226 K. M. Kim, J.-C. Kim and K. S. Ryu, *Macromol. Mater. Eng.*, 2006, **291**, 1495–1502.
227 K.-S. Park, J. H. Cho, K. Shanmuganathan, J. Song, J. Peng, M. Gobet, S. Greenbaum, C. J. Ellison and J. B. Goodenough, *J. Power Sources*, 2014, **263**, 52–58.

228 F. Mizuno, A. Hayashi, K. Tadanaga and M. Tatsumisago, *Adv. Mater.*, 2005, **17**, 918–921.
229 R. Murugan, V. Thangadurai and W. Weppner, *Angew. Chem., Int. Ed.*, 2007, **46**, 7778–7781.
230 R. Kanno and M. Maruyama, *J. Electrochem. Soc.*, 2001, **148**, A742–A746.
231 J. Y. Song, Y. Y. Wang and C. C. Wan, *J. Electrochem. Soc.*, 2000, **147**, 3219–3225.
232 J. S. Tockchom, N. Gupta and B. Kumar, *J. Electrochem. Soc.*, 2008, **155**, A915–A920.
233 G. Sahu, E. Rangasamy, J. Li, Y. Chen, K. An, N. Dudney and C. Liang, *J. Mater. Chem. A*, 2014, **2**, 10396–10403.
234 L. Edman, A. Ferry and M. M. Doeff, *J. Mater. Res.*, 2000, **15**, 1950–1954.
235 A. Hayashi, K. Minami, F. Mizuno and M. Tatsumisago, *J. Mater. Sci.*, 2008, **43**, 1885–1889.
236 J. W. Fergus, *J. Power Sources*, 2010, **195**, 4554–4569.
237 Z. Jin, K. Xie, X. Hong, Z. Hu and X. Liu, *J. Power Sources*, 2012, **218**, 163–167.
238 K. Takada, N. Aotani and S. Kondo, *J. Power Sources*, 1993, **43**, 135–141.
239 N. Kamaya, K. Homma, Y. Yamakawa, M. Hirayama, R. Kanno, M. Yonemura, T. Kamiyama, Y. Kato, S. Hama, K. Kawamoto and A. Mitsui, *Nat. Mater.*, 2011, **10**, 682–686.
240 F. Croce, G. B. Appetecchi, L. Persi and B. Scrosati, *Nature*, 1998, **394**, 456–458.
241 A. Kuhn, O. Gerbig, C. Zhu, F. Falkenberg, J. Maier and B. V. Lotsch, *Phys. Chem. Chem. Phys.*, 2014, **16**, 14669–14674.
242 I. Yoshiyuki, L. Chen, I. Mitsuru, N. Tesuro, U. Takashi, I. Hiromasa and W. Masataka, *Solid State Commun.*, 1993, **86**, 689–693.
243 T. Zhang, N. Imanishi, Y. Shiminishi, A. Hirano, Y. Takeda, O. Yamamoto and N. Sammes, *Chem. Commun.*, 2010, **46**, 1661–1663.
244 W. H. Meyer, *Adv. Mater.*, 1998, **10**, 439–448.
245 V. Aravindan, J. Gnanaraj, S. Madhavi and H.-K. Liu, *Chem. – Eur. J.*, 2011, **17**, 14326–14346.
246 J. B. Goodenough and K.-S. Park, *J. Am. Chem. Soc.*, 2013, **135**, 1167–1176.
247 J. Ibarra, A. Várez, C. León, J. Santamaría, L. M. Torres-Martínez and J. Sanz, *Solid State Ionics*, 2000, **134**, 219–228.
248 Y. Inaguma and M. Itoh, *Solid State Ionics*, 1996, **86–88**, 257–260.
249 J. Trevey, J. S. Jang, Y. S. Jung, C. R. Stoldt and S.-H. Lee, *Electrochem. Commun.*, 2009, **11**, 1830–1833.
250 K. Minami, A. Hayashi, S. Ujiie and M. Tatsumisago, *J. Power Sources*, 2009, **189**, 651–654.
251 M. Tatsumisago, F. Mizuno and A. Hayashi, *J. Power Sources*, 2006, **159**, 193–199.
252 T. Minami, A. Hayashi and M. Tatsumisago, *Solid State Ionics*, 2006, **177**, 2715–2720.
253 M. Barré, F. Le Berre, M.-P. Crosnier-Lopez, C. Galven, O. Bohnké and J.-L. Fourquet, *Ionics*, 2009, **15**, 681–687.
254 N. V. Kosova, E. T. Devyatkina, A. P. Stepanov and A. L. Buzlukov, *Ionics*, 2008, **14**, 303–311.
255 B. Kumar, D. Thomas and J. Kumar, *J. Electrochem. Soc.*, 2009, **156**, A506–A513.
256 X. Xu, Z. Wen, Z. Gu, X. Yang, J. Zhang and Z. Gu, *Solid State Ionics*, 2006, **177**, 2611–2615.
257 C. Ma, E. Rangasamy, C. Liang, J. Sakamoto and K. L. More, *Angew. Chem., Int. Ed.*, 2015, **54**, 129–133.
258 S. D. Jackman and R. A. Cutler, *J. Power Sources*, 2013, **230**, 251–260.
259 T. Yang, X. Liu, L. Sang and F. Ding, *J. Power Sources*, 2013, **244**, 43–49.
260 X. Wang, Q. Qu, Y. Hou, F. Wang and Y. Wu, *Chem. Commun.*, 2013, **49**, 6179–6181.
261 Z. Chang, Y. Yang, M. Li, X. Wang and Y. Wu, *J. Mater. Chem. A*, 2014, **2**, 10739–10755.
262 Y. Hou, X. Wang, Y. Zhu, C. Hu, Z. Chang, Y. Wu and R. Holze, *J. Mater. Chem. A*, 2013, **1**, 14713–14718.
263 F. Ding, W. Xu, G. L. Graff, J. Zhang, M. L. Sushko, X. Chen, Y. Shao, M. H. Engelhard, Z. Nie, J. Xiao, X. Liu, P. V. Sushko, J. Liu and J.-G. Zhang, *J. Am. Chem. Soc.*, 2013, **135**, 4450–4456.
264 C. Zu and A. Manthiram, *J. Phys. Chem. Lett.*, 2014, **5**, 2522–2527.
265 G. Zheng, S. W. Lee, Z. Liang, H.-W. Lee, K. Yan, H. Yao, H. Wang, W. Li, S. Chu and Y. Cui, *Nat. Nanotechnol.*, 2014, **9**, 618–623.
266 D. Aurbach, E. Pollak, R. Elazari, G. Salitra, C. S. Kelley and J. Affinito, *J. Electrochem. Soc.*, 2009, **156**, A694–A702.
267 Y. Lu, Z. Tu and L. A. Archer, *Nat. Mater.*, 2014, **13**, 961–969.
268 C. Huang, J. Xiao, Y. Shao, J. Zheng, W. D. Bennett, D. Lu, L. V. Saraf, M. Engelhard, L. Ji, J. Zhang, X. Li, G. L. Graff and J. Liu, *Nat. Commun.*, 2014, **5**, 3015.
269 M. Buonaiuto, S. Neuhold, D. J. Schroeder, C. M. Lopez and J. T. Vaughey, *ChemPlusChem*, 2015, **80**, 363–367.
270 Y. Y. Zhang, Y. Y. Sun, S. X. Du, H.-J. Gao and S. B. Zhang, *Appl. Phys. Lett.*, 2012, **100**, 091905.
271 S. Wang, L. Wang, K. Zhang, Z. Zhu, Z. Tao and J. Chen, *Nano Lett.*, 2013, **13**, 4404–4409.
272 E. Castillo-Martínez, J. Carretero-González and M. Armand, *Angew. Chem., Int. Ed.*, 2014, **53**, 5341–5345.
273 L. M. Zhu, W. Shi, R. R. Zhao, Y. L. Cao, X. P. Ai, A. W. Lei and H. X. Yang, *J. Electroanal. Chem.*, 2013, **688**, 118–122.
274 X. Han, G. Qing, J. Sun and T. Sun, *Angew. Chem., Int. Ed.*, 2012, **51**, 5147–5151.
275 Y. Zhao, S. Si, L. Wang, P. Tang and H. Cao, *J. Electrochem. Soc.*, 2014, **161**, A330–A335.
276 R. S. Stojanovic and A. M. Bond, *Anal. Chem.*, 1993, **65**, 56–64.
277 N. G. Connelly and W. E. Geiger, *Chem. Rev.*, 1996, **96**, 877–910.
278 S. Gu, K. Gong, E. Z. Yan and Y. Yan, *Energy Environ. Sci.*, 2014, **7**, 2986–2998.
279 W. Wang, Q. Luo, B. Li, X. Wei, L. Li and Z. Yang, *Adv. Funct. Mater.*, 2013, **23**, 970–986.
280 M. Park, J. Ryu, Y. Kim and J. Cho, *Energy Environ. Sci.*, 2014, **7**, 3727–3735.
281 P. F. Driscoll, E. Deunf, L. Rubin, J. Arnold and J. B. Kerr, *J. Electrochem. Soc.*, 2013, **160**, G3152–G3158.

